OLD DOMINION UNIVERSITY RESEARCH FOUNDATION

DEPARTMENT OF MECHANICAL ENGINEERING AND MECHANICS
SCHOOL OF ENGINEERING
OLD DOMINION UNIVERSITY
NORFOLK, VIRGINIA

SIGNIFICANCE OF SHOCK AND BODY SLIP CONDITIONS ON JOVIAN ENTRY HEATING

By

S. N. Tiwari
Principal Investigator

and

K. Y. Szema

Progress Report
For the period August to December 1978

Prepared for the
National Aeronautics and Space Administration
Langley Research Center
Hampton, Virginia

Under
Research Grant NSG 1492
Randolph A. Graves, Jr., Technical Monitor
Space Systems Division

January 1979

DEPARTMENT OF MECHANICAL ENGINEERING AND MECHANICS
SCHOOL OF ENGINEERING
OLD DOMINION UNIVERSITY
NORFOLK, VIRGINIA

SIGNIFICANCE OF SHOCK AND BODY SLIP CONDITIONS ON JOVIAN ENTRY HEATING

By

S. N. Tiwari
Principal Investigator

and

K. Y. Szema

Progress Report
For the period August to December 1978

Prepared for the
National Aeronautics and Space Administration
Langley Research Center
Hampton, Virginia 23665

Under
Research Grant NSG 1492
Randolph A. Graves, Jr., Technical Monitor
Space Systems Division

Submitted by the
Old Dominion University Research Foundation
P.O. Box 6369
Norfolk, Virginia 23508

January 1979

FOREWORD

This report constitutes a part of the work completed on the research project entitled "Influence of Precursor Heating on Nonequilibrium Viscous Flow Around a Jovian Entry Body." The work was supported by the NASA-Langley Research Center (Aerothermodynamics Branch of the Space Systems Division) through research grant NSG 1492. The grant was monitored by Dr. Randolph A. Graves, Jr. of the Space Systems Division.

TABLE OF CONTENTS

LIST OF TABLES

LIST OF FIGURES

SIGNIFICANCE OF SHOCK AND BODY SLIP CONDITIONS ON JOVIAN ENTRY HEATING

By

S. N. Tiwari[1] and K. Y. Szema[2]

SUMMARY

The influence of the body and shock slip conditions on the heating of a Jovian entry body is investigated. The flow in the shock lazer is considered to be axisymmetric, steady, laminar, viscous, and in chemical equilibrium. Realistic thermophysical and step-function spectral models are employed and results are obtained by implicit finite-difference and iterative procedures. The free-stream conditions correspond to a typical Jovian entry trajectory point. The results indicate that the effect of the slip conditions is significant when the altitudes are higher than 225 km and that the contribution of a radiative heat-flux term in the energy equation should not be neglected at any altitude.

1. INTRODUCTION

A space vehicle entering a planetary atmosphere encounters a wide range of flow conditions ranging from free molecular flow at high altitudes to continuum flow at low altitudes. Since experimental facilities cannot adequately simulate conditions expected during entry into the outer planetary atmospheres, most of the required information must be obtained from theoretical studies.

It is very well documented in the literature that the degree of rarefaction of a flow is measured by the Reynolds number. Therefore, for a fixed

---

[1] Professor, Department of Mechanical Engineering and Mechanics, Old Dominion University, Norfolk, Virginia 23508.

[2] Graduate Research Assistant, Department of Mechanical Engineering and Mechanics, Old Dominion University, Norfolk, Virginia 23508.

blunt body at low altitudes where the Reynolds number is high, the flow will behave like an ordinary viscous flow which lies within the scope of the Navier-Stokes equations. At higher altitudes, where the Reynolds number is low, the theory of free molecular flow can be used. The transition zone between these two regions has been divided into several subregions which are discussed in greater detail by Hays and Probstein (ref. 1) and Probstein (ref. 2), and Cheng (ref. 3) has provided different methods of solution valid within each region. In the continuum range, the flow phenomena are investigated through use of the Navier-Stokes equations. In the transition range (from the continuum end), however, use of the Navier-Stokes equations is still justified for the main flow field, but the boundary conditions cannot be satisfied in the usual manner. Thus, the characteristic feature of flow of a slightly rarefied gas, which sharply distinguishes it from the continuum flow, is the change in the boundary conditions at the body surface and the shock wave (refs. 4-9).

The hypersonic entry conditions encountered by a probe entering Jupiter's atmosphere are such that the heating environment is extremely severe. The initial onset of heating is convective, followed by a much shorter yet more intense radiative heating pulse. At the onset of the convective heating pulse, the flow regime is such that the Reynolds numbers are small (ref. 10). For this type of flow, therefore, the slip boundary conditions (both shock and wall) become important. Thus, it is desirable to investigate the impact of slip boundary conditions on flow phenomena around a Jovian entry body for a currently envisioned Jupiter entry trajectory. It is particularly important to examine the significance of the shock slip boundary conditions (as opposed to the conventional Rankine-Hugoniot relations) on convective heating and the onset of radiative heating. The initial portion of the radiative heating pulse may be extremely sensitive to the shock boundary conditions used since the radiation is very sensitive to the chemical composition and temperature of the shock layer. Therefore, it is important to investigate how sensitive both the convective and radiative heating are to slip boundary conditions.

Steady, viscous shock-layer conservation equations which are used to describe a reacting multicomponent gas mixture flow field can be found in the literature (refs. 11-14). These equations are obtained by retaining terms up

to second order in the Reynolds number parameter. Because of the low Reynolds number at higher entry altitudes, these equations should be used with modified boundary conditions at both the body and shock. Rott and Lenard (ref. 4) have shown that the effects of velocity slip and temperature jump on the surface cannot be neglected in comparison with other low Reynolds number corrections. A semi-macroscopic argument which leads to simple expressions for the velocity slip and temperature jump is given in references 4 and 7. Since the viscous model does not satisfactorily describe a low Reynolds number flow, we may no longer consider the shock as a discontinuity as described by the Hugoniot relations. Instead of using the Rankine-Hugoniot conditions as the boundary conditions at the shock wave, Probstein and Pan (refs. 5 and 6) introduced the concept of "shock-wave slip" as an interpretation of the transported effects behind the shock. Although it is necessary to consider the effects of transport and thickness, the shock may still be considered thin in comparison with the shock layer.

The purpose of this study, therefore, is to investigate the sensitivity of both the shock and body slip boundary conditions on convective and radiative heating for an early (high-altitude) portion of a Jupiter atmospheric entry trajectory. A finite-difference method, presented by Moss (ref. 12) for the Earth's atmosphere, is used here for the hydrogen-helium atmosphere. By introducing appropriate thermodynamic and spectral information, proper modifications are made in governing equations and boundary conditions. Basic formulation of the problem is presented in section 3. Boundary conditions are discussed in section 4. Thermodynamics and transport properties are given in section 5, equilibrium chemical composition and surface convective heat transport in section 6, and radiative transport equations in section 7. The method of solution is discussed in section 8, and the results are presented in section 9.

2. LIST OF SYMBOLS

B_ν	Planck blackbody radiation function, erg/cm^2
C_p^*	specific heat at constant pressure, erg/g-K
C_p	$C_p^*/C_{p\infty}^*$

C_α mass fraction of species α

$E_n(t)$ exponential integral function of order n

H defined quantity, $h + u^2/2$

H_T total enthalpy, $h + (u^2 + v^2)/2$

h^* specific enthalpy, erg/g

h h^*/V_∞^{*2}, also Planck constant (= 6.6256E27 erg-sec)

I_ν specific intensity, erg/cm^2

J_i diffusion mass flux of species i

K^* thermal conductivity, erg/sec-cm-K

K $K^*/\mu^*_{ref} C^*_{p\infty}$

k Boltzmann constant (= 1.38E-16 erg/K)

M molecular weight, g/mole

M_α molecular weight of species α, g/mole

p^* pressure, dyne/cm^2

p $p^*/\rho^*_\infty V^{*2}_\infty$

Pr Prandtl number

q_R net radiative heat flux, erg/cm^2-sec

q_R^+ radiative heat flux toward shock

q_R^- radiative heat flux toward body

R universal gas constant

R_b^* radius of the body, cm

R_n^* body nose radius curvature, cm

r^* radius measured from axis of symmetry to point on body surface, cm

T^* temperature, K

T $T^*/\rho^*_\infty V^{2*}_\infty$

u^*	velocity component tangent to the body surface, cm/sec
u	u^*/V_∞^*
V_∞^*	free-stream velocity cm/sec
v^*	velocity component normal to the body surface, cm/sec
v	v^*/V_∞^*
X^*	coordinate measured along the body surface, cm
Y^*	coordinate measured normal to the body surface, cm
α	shock angle defined in figure 1
ε	surface emittance
η	transformed n coordinate, y/y_s
κ	body curvature ($= \kappa^* R_n^*$), $\kappa^* = 1/R_b$
κ_ν	spectral absorption coefficient
μ	nondimensional viscosity, μ^*/μ^*_{ref}
μ^*	viscosity, g/cm-sec
μ^*_{ref}	reference viscosity at temperature $V_\infty^{*2}/C_{p\infty}^*$, g/cm-sec
ν	frequency
ξ	coordinate measured along the body surface, $\xi = X$
ρ	nondimensional density, ρ^*/ρ_∞^*
ρ^*	density, g/cm^3
τ	optical thickness

SUPERSCRIPTS:

*	dimensional quantities
-	transformed quantities defined by equation (7.1)
'	shock surface curvilinear orthogonal coordinates system

SUBSCRIPTS:

s	shock value
b	body surface
i	species
∞	free-stream value

3. BASIC FORMULATION

The physical model and coordinate system for a Jovian entry body are shown in figure 1. The nondimensional conservation equations for the reacting multicomponent gas mixture in the shock layer can be written as (refs. 12-14):

Continuity:

$$(\partial/\partial x)[(r + y\cos\theta)\rho u] + (\partial/\partial y)(\Gamma\zeta\rho v) = 0 \tag{3.1}$$

X-momentum:

$$\rho[(u/\Gamma)(\partial u/\partial x) + v\,(\partial u/\partial y) + uv\kappa/\Gamma + \Gamma^{-1}(\partial\rho/\partial x) = \varepsilon^2[(\partial/\partial y)\,(\mu\psi) + \mu(2\kappa/\Gamma + \cos\theta/\zeta) + \psi] \tag{3.2}$$

Y-momentum:

$$\rho[(u/\Gamma)(\partial v/\partial x) + v(\partial v/\partial y) - u^2\kappa/\Gamma] + \partial p/\partial y \doteq 0 \tag{3.3a}$$

If thin shock layer is assumed, the above equation becomes

$$\rho u^2\kappa/\Gamma = \partial p/\partial y \tag{3.3b}$$

Energy:

$$\rho[(u/\Gamma)(\partial H/\partial x) + v(\partial H/\partial y)] - v(\partial p/\partial y) + \rho\kappa u^2 v/\Gamma = \varepsilon^2[\partial\phi/\partial y + (\kappa/\Gamma + \cos\theta/\zeta)\phi] - \operatorname{div} \underset{\sim}{q}_R \tag{3.4}$$

where

$$\left.\begin{aligned}
&\Gamma = 1 + y.\kappa,\ \zeta = r + y\cos\theta,\ H = h + u^2/2 \\
&\varepsilon = u^*_{ref}/(\rho^*_\infty V^*_\infty R_N)^{\frac{1}{2}},\ \psi = \partial u/\partial y - u\kappa/\Gamma \\
&\phi = (u/Pr)\left[\partial H/\partial y - \sum_{i=1}^{N} h_i(\partial C_i/\partial y) - (Pr/\mu)\sum_{i=1}^{N} h_i J_i\right. \\
&\qquad \left. + (Pr - 1)\mu(\partial u/\partial y) - Pr\kappa u^2/\Gamma\right]
\end{aligned}\right\} \quad (3.5)$$

The quantity J_i appearing in the energy equation represents the mass flux relative to the mass average velocity and is given by the relation:

$$J_i = -(\mu/Pr)\left[\sum_{K=1}^{NI} \bar{b}_{iK}(\partial C_K/\partial y) + (L_i^T/T)(\partial T/\partial y)\right] \quad (3.6a)$$

where

$$\bar{b}_{iK} = \begin{cases} Le_i, & i = K \\ \Delta\bar{b}_{iK}, & i \neq K \end{cases}$$

$$Le_i = \sum_{\substack{j=1 \\ j\neq 1}}^{NI}\left(\frac{C_j}{M_j}\right) \Bigg/ \sum_{\substack{j=1 \\ j\neq i}}^{NI}\left(C_j/M_j L_{ij}\right)$$

$$\Delta\bar{b}_{iK} = Le_i - \left\{(M_i/M)Le_{iK} + [1-(M_i/M_K)]\sum_{j=1}^{NI} Le_{ij}C_j\right\}$$

The last term in equation (3.6a) represents the contribution of thermal diffusion. The quantity Le_{ij} represents the multicomponent Lewis number, and L_{ij} represents the binary Lewis Semenov numbers. If thermal diffusion can be neglected and L_{ij} can be taken as constant for all species, then equation (3.6a) reduces to

$$J_i = -(\mu/Pr)L_{ij}(\partial C_i/\partial y) \quad (3.6b)$$

In the present study, use is made of equation (3.6b), and the value for L_{ij} is taken to be 1.1 (ref. 14).

The expression for the equation of state for a hydrogen/helium mixture is given by Zoby et al. (ref. 15) as

$$T^* = C_T\left[(p^*/1013250)^{\ell}/(\rho^*/0.001292)^{k}\right] \tag{3.7a}$$

$$H^* = C_H\left[(p^*/1013250)^{m}/(\rho^*/0.001292)^{n}\right](RT_o/M) \tag{3.7b}$$

where

$$k = 0.65206 - 0.04407\ \ell n\left(X_{H_2}\right)$$

$$\ell = 0.67389 - 0.04637\ \ell n\left(X_{H_2}\right)$$

$$m = 0.95252 - 0.1447\ \ell n\left(X_{H_2}\right)$$

$$n = 0.97556 - 0.16149\ \ell n\left(X_{H_2}\right)$$

$$U_t = V_\infty \sin\theta\left[1 + 0.7476\left(1-X_{H_2}\right)\right]$$

$$CTU = -545.37 + 61.608\ U_t - 22459\ U_t^2 + 0.039922\ U_t^3 - 0.00035148\ U_t^4 + 0.0000012361\ U_t^5$$

$$CHU = 5.6611 - 0.52661\ U_t + 0.020376\ U_t^2 - 0.00037861\ U_t^3 + 0.0000034265\ U_t^4 - 0.000000012206\ U_t^5$$

$$C_T = CTU + 61.2\left(1 - X_{H_2}\right)$$

$$C_H = CHU - 0.3167\left(1 - X_{H_2}\right)$$

and X_{H_2} represents the mole fraction of H_2.

The set of governing equations presented above has a hyperbolic-parabolic nature. If the thin shock-layer approximation is used, the resulting set of equations is parabolic. An iteration method is used to remove this approximation, and this is discussed in section 8, "Method of Solution."

In order to solve the above set of governing equations, it is essential to specify appropriate boundary conditions at the body surface and at the shock. These are discussed, in detail, in the next section.

The heat transferred to the wall due to conduction and diffusion is referred to here as the convective heat flux and is given by the relation:

$$q_{c,w} = - \varepsilon^2 \left[-K(\partial T/\partial y) + \sum_{i=1}^{N} J_i h_i \right] \tag{3.8}$$

4. BOUNDARY CONDITIONS

As pointed out earlier, the slip boundary conditions are not important at low altitudes, but they cannot be neglected at higher altitudes. Since both the slip and no-slip conditions have been used in this study, they will be discussed separately in this chapter.

4.1. No-Slip Boundary Conditions

At the body surface (wall), no velocity slip and no temperature jump are assumed. Consequently, the velocities at the surface are

$$v = 0 \tag{4.1}$$

$$u = 0 \tag{4.2}$$

The wall temperature for this study is specified as

$$T_w = \text{constant} \tag{4.3}$$

The Rankine-Hugoniot relations are used to determine the flow properties immediately behind the shock. The nondimensional form of the shock relations can be written as (ref. 14):

Continuity:

$$\rho_{s-} v'_{s-} = - \sin \alpha \tag{4.4}$$

Momentum:

$$u'_{s-} = \sin \alpha \tag{4.5}$$

$$p_{s-} = p_{s+} + \sin^2 \alpha(1 - 1/\rho_{s-}) \tag{4.6}$$

Energy:

$$h_{s-} = h_{s+} + (\sin^2 \alpha/2)(1 - 1/\rho^2_{s-}) \tag{4.7}$$

where α is shown in figure 1, and u'_s and v'_s are velocity components expressed in a shock-oriented coordinate system. The relations for u_s and v_s in the body-oriented coordinate system can be written as

$$u_s = u'_s \sin(\alpha + \beta) + v'_s \cos(\alpha + \beta) \tag{4.8}$$

$$v_s = -u'_s \cos(\alpha + \beta) + v'_s \sin(\alpha + \beta) \tag{4.9}$$

where angle β is indicated in figure 1.

4.2. Slip Boundary Conditions

The name "slip boundary condition," as used in this study, implies both the body-slip and shock-slip conditions. These are discussed separately in the following subsections.

4.2.1. Body (or surface) slip conditions. - Shidlovkey (ref. 7) has shown that at the body surface the velocity slip and temperature jump conditions are of the same order as the Knudsen number. The Knudsen number, Kn, is defined as the ratio of the particle's mean free path ℓ and the characteristic dimension L of the body (i.e., $Kn = \ell/L$). The ordinary boundary conditions (which correspond to continuum conditions) are obtained when $Kn \to 0$. However, for the transitional range {i.e., for $Kn \to 0(1)$}, in order to be consistent with the Navier-Stokes equations of motion, a linear relation between the conditions at the wall and the flow should be assumed. This can be done by a semi-macroscopic argument which leads to the simple expression for velocity slip and temperature jump as (refs. 4, 7, 9, 16, and 17)

$$u = \varepsilon^2 A_1 (\mu/p)(p/\rho)^{\frac{1}{2}}(\partial u/\partial y) \tag{4.10}$$

$$T = T_w + \varepsilon^2 A_2 (K/p)(p/\rho)^{\frac{1}{2}}(\partial T/\partial y) \tag{4.11}$$

$$v = 0 \tag{4.12}$$

where A_1 and A_2 are constants and are given by

$$A_1 = [(2 - \sigma_1)/\sigma_1](\pi/2)^{\frac{1}{2}}, \quad A_2 = [(2 - \sigma_2)/\sigma_2](15/8)(\pi/2)^{\frac{1}{2}}$$

The terms σ_1 and σ_2 are slip and thermal accommodation coefficients respectively and are dependent on the nature of the surface and fluid. However, in actual flight conditions both σ_1 and σ_2 are expected to be 1. The concentration slip was introduced by Davis (ref. 11) and can be written as

$$C_i = C_{ie} + \varepsilon^2 (\pi M_i/M_{mix})^{\frac{1}{2}}[(2-\gamma_w)/\gamma_w](F_D/p)(p/\rho)^{\frac{1}{2}} \frac{\partial C_i}{\partial y} \tag{4.13}$$

where γ_w is the recombination coefficient and F_D is the diffusion coefficient.

4.2.2. Shock slip conditions.- As pointed out earlier, in evaluating the boundary conditions at the shock wave, the classical Rankine-Hugoniot relations cannot be used when the Reynolds number is low; the transport and thickness effects should be considered in finding the appropriate relations. The transport and thickness effects are discussed here separately.

For the present study, the shock may still be considered thin when compared to the thickness of the viscous shock layer. As such, the thin-layer approximations $(\partial/\partial X') << (\partial/\partial y')$ and $y'/R_s << 1$ can be used in the shock transition zone. The notations x' and y' are used for the shock surface curvilinear orthogonal coordinates in figure 1. By using Stokes assumption and applying the hypersonic thin-layer approximation, the governing equations for the shock transition zone can be expressed as (ref. 18)

Continuity:

$$\rho_\infty^* V_\infty^* = \rho^* v^* \tag{4.14}$$

x'-momentum:

$$p^* + \rho_\infty^* V_\infty^* v^* - \left(\frac{4}{3}\right)\mu^* \frac{\partial v^*}{\partial y^*} = \rho_\infty^* V_\infty^{*2} \tag{4.15}$$

y'-momentum:

$$\rho_\infty^* V_\infty^* u^* - \mu^* \frac{\partial u^*}{\partial y^*} = \rho_\infty^* V_\infty^* U_\infty^* \tag{4.16}$$

Energy:

$$\rho_\infty^* V_\infty^* H^* - (\mu/Pr) \frac{\partial}{\partial y^*} \left[H-(1-P_r)u^{*2}/2 - (1 - \frac{4}{3} P_r^*)v^{*2}/2\right] = \rho_\infty^* V_\infty^* H_\infty^* \tag{4.17}$$

where $H^* = h^* + (u^{*2} + v^{*2})/2$.

At the downstream edge of the transition zone, both v and $(4/3)[\mu(\partial v/\partial y)]$ are reduced to high-order quantities under a high shock compression ratio. Therefore, a set of modified transport boundary conditions immediately behind the shock can be written as

$$\rho_\infty^* V_\infty^* = \rho_s^* v_s^* \tag{4.18}$$

$$\rho_\infty^* V_\infty^* u_s^* - \mu_s^* (\partial u^*/\partial y)_s = \rho_\infty^* v_\infty^* U_\infty^* \tag{4.19}$$

$$p_s^* + \rho_\infty^* V_\infty^* v_s^* = p_\infty^* + \rho_\infty^* V_\infty^{*2} \tag{4.20}$$

$$\rho_\infty^* V_\infty^* (H_s^* - H_\infty^*) = \left\{(\mu_s^*/Pr) \frac{\partial}{\partial y} [H^* - (1-Pr)u^{*2}/2]\right\} \tag{4.21}$$

By introducing $v = \bar{v} \sin \alpha$, $u = \bar{v} \cos \alpha$ and nondimensionalizing all the quantities, the final modified Rankine-Hugoniot conditions are obtained as

$$\rho_s v_s' = \sin \alpha \tag{4.22}$$

$$u_s' = \cos \alpha - (\varepsilon^2 \mu_s / \sin \alpha)(\partial u_s'/\partial y') + \cos \alpha \tag{4.23}$$

$$p_s = p_\infty + \sin^2 \alpha (1 - 1/\rho_s) \tag{4.24}$$

$$h_s = h_\infty - (\epsilon^2 \mu_s / Pr \sin\alpha)\,(\partial h/\partial y') + \frac{1}{2}\left[(u_s' - \cos\alpha)^2 + \sin^2\alpha - v_s'^2\right] \tag{4.25}$$

$$u_s' \sin(\alpha + \beta) + v_s' \cos(\alpha + \beta) = u_s \tag{4.26}$$

$$-u_s' \cos(\alpha + \beta) + v_s' \sin(\alpha + \beta) = v_s \tag{4.27}$$

The shock conditions, which include the thickness effect, have been discussed in references 19 and 20. The detailed analysis procedure is rather lengthy and will not be given here. Only an outline of the procedure and applications to the oblique shock condition will be discussed. The oblique shock structure is analyzed by using a boundary-layer technique (method of matched asymoptotic expansions, ref. 20) and in this manner the boundary conditions at the shock wave are determined. The shock slip effect comes out automatically without the need for the artificial separation. The following expansions are now assumed for the dependent variables:

$$u^{*'}(x',y',\alpha) = u^{*'(0)} + \alpha' u^{*'(1)} + O(\alpha'^2) \tag{4.28}$$

$$v^{*'}(x',y',\alpha) = v^{*'(0)} + \alpha' v^{*'(1)} + O(\alpha'^2) \tag{4.29}$$

$$m^*(x',y',\alpha) = m^{*'(0)} + \alpha' m^{*(1)} + O(\alpha'^2) \tag{4.30}$$

$$\rho^*(x',y',\alpha) = \rho^{*(0)} + \alpha' \rho^{*(1)} + O(\alpha'^2) \tag{4.31}$$

In the above equations, (0) and (1) denote zero and first order quantities, respectively. The term α is the inverse Reynolds number.

The zero-order shock structure is obtained by substituting the expansion (4.28) to (4.31) into the Navier-Stokes equations. The solution can be written as

$$u^{*'(0)} + \bar{V}_\infty^* \cos\alpha \tag{4.32}$$

$$\rho^{*(0)} = -(\rho_\infty^* \bar{V}_\infty^* \sin\alpha)/v^{*'(0)} \tag{4.33}$$

$$p_\infty^{*(0)} = p_\infty^* + \rho_\infty^* V_\infty^{*2} \sin^2 \alpha - \rho^{*(0)} v^{*\prime 2(0)} - [(r + 1)/2r]$$

$$\cdot [\rho_\infty^* V_\infty^{*\prime} \sin \alpha / v^{*\prime(0)}](v^{*\prime(0)} + V_\infty^* \sin \alpha)$$

$$\cdot \{v^{*\prime(0)} + [(r - 1)/(r + 1)] K_1 \bar{V}_\infty^* \sin \alpha\} \tag{4.34}$$

$$h^{*(0)} = \frac{1}{2}(K_1 \bar{V}^{*2} \sin \alpha - v^{*\prime 2(0)}) \tag{4.35}$$

where

$$K_1 = 1 + 2/[(r - 1)\, M_\infty^2 \sin^2 \alpha]$$

The first-order shock structure is analyzed by introducing the series into the integrated mass, momentum, and energy-flux relations of shock. The first-order shock-jump condition can be found from reference 6, and this is given by

$$[\rho u' v']_{(1)} = \alpha\{(\mu/\alpha)[\partial v'/\partial x' + \partial u'/\partial y' - (u'/r)] - (\partial/\partial x')$$

$$\cdot [(2\mu/3\alpha')\partial v'/\partial s + \rho] - (\partial/\partial x')(\rho^* U_\infty^{\prime 2})\} \tag{4.36}$$

$$[p + \rho v'^2]_{(1)} = \alpha\{(4\mu/\overline{3\alpha})\partial v'/\partial y' - (2\mu/3\alpha')(\partial u'/\partial x' + v'/r)$$

$$+ (1/r)[p + (2\mu/3\alpha')\partial v'/\partial s]^* + (\rho^* U_\infty^{\prime 2}/r)\} \tag{4.37}$$

$$\left\{[h + \frac{1}{2}(u'^2 + v'^2)]\rho v'\right\}_{(1)} = \alpha\{u'(\mu/\alpha)(\partial v'/\partial x' + \partial u'/\partial y' - u'/r)$$

$$+ [(4\mu/3\alpha')\partial v'/\partial y' - (2\mu/3\alpha')(\partial u'/\partial x' + v'/r)]$$

$$+ (\mu/\alpha' Pr)\partial h/\partial y' - (\partial/\partial x')[h + \frac{1}{2}(u'^2 + v'^2)]\rho^* U_\infty'$$

$$- (\partial/\partial x')[(2\mu/3\alpha)\partial v'/\partial s]^* U_\infty'\} \tag{4.38}$$

In the above equations, the subscript 1 is used to indicate the shock-jump condition to first order. The usual Rankine-Hugoniot conditions can be

obtained by setting the right-hand side of the above equation equal to zero. The first-order corrections to the shock-jump conditions can be obtained by retaining the first-order terms in these equations. The details of the calculation procedure can be found in reference 5, and the results may be written as

$$u^{*\prime(1)} = \frac{-\mu_s^*}{\alpha' \rho_\infty^* \bar{V}_\infty^* \sin\alpha} \left(\frac{\partial u^{*\prime}}{\partial y'}\right)_s - \frac{8}{3}\frac{r}{r+1}\frac{\bar{V}_\infty^*}{\varepsilon K_1 \sin\alpha} g(K_1, r) \tag{4.39}$$

$$h^{*\prime(1)} = \frac{8}{3}\frac{r}{r+1}\frac{\bar{V}_\infty^{*2}}{\varepsilon K_1 \sin\alpha} g(K_1, r)\left[\frac{1}{4} + \frac{rK_1}{r+1}\right] \tag{4.40}$$

$$g(K_1, r) = \ln \frac{(r+3)K_1 - 2(r+1)\sqrt{K_1(K_1 - 1)}}{(r+3)K_1 + 2(r+1)\sqrt{K_1(K_1 - 1)}} + \frac{2\sqrt{K_1}}{\sqrt{K_1 - 1}} \tag{4.41}$$

From the above treatment and development presented in reference 5, it is evident that the thickness effect is of higher order in the Reynolds number parameter. As such, this effect could be neglected in a first-order treatment of the shock-slip conditions.

5. THERMODYNAMIC AND TRANSPORT PROPERTIES

Thermodynamic properties for specific heat, enthalpy, and free energy, and transport properties for viscosity and thermal conductivity are required for each species considered in the shock-layer gas. The general expressions for total enthalpy, specific enthalpy, and specific heat at constant pressure are given respectively by

$$H_T = h + \frac{u^2 + v^2}{2} \tag{5.1}$$

$$h = \sum x_i h_i = \left[\sum (C_\alpha / M_\alpha) h_\alpha\right] M_{mix} \tag{5.2}$$

$$C_p = \sum x_i C_{Pi} \tag{5.3}$$

With x_i representing the mole fraction of the ith species the expressions for h_i and C_{Pi} are found from references 21 and 22 as

$$h_i = RT[a_1 + (a_2/2)T + (a_3/3)T^2 + (a_4/4)T^3 + (a_5/5)T^4 + a_6/T] \tag{5.4}$$

$$C_{pi} = R(a_1 + a_2T + a_3T^2 + a_4T^3 + a_5T^4 \tag{5.5}$$

where R is the universal gas constant (=1.98726 cal/mole - K) and T is the local fluid temperature in K. For different species, values of the polynomial constants a_1, a_2,...a_6 are given in reference 21, and for species under present investigation they are listed in table 1.

For the shock-layer gas, the mixture viscosity and thermal conductivity are obtained by using the semi-empirical formulas of Wilke (ref. 23) as

$$\mu = \sum_{i=1}^{N}\left[x_i\mu_i/\left(\sum_{j=1}^{N} x_j\phi_{ij}\right)\right] \tag{5.6}$$

$$K = \sum_{i=1}^{N}\left[x_iK_i/\left(\sum_{j=1}^{N} x_j\phi_{ij}\right)\right] \tag{5.7}$$

where

$$\phi_{ij} = \left[1 + (\mu_i/\mu_j)^{1/2}(M_j/M_i)^{1/4}\right]^2/\left\{\sqrt{8}\left[1 + (M_i/M_j)\right]\right\}^{1/2}$$

and M_i is the molecular weight of species i. For hydrogen/helium species, specific relations for viscosity and thermal conductivity are given in references 24 and 25. The viscosity of H_2 and He, as a function of temperature, can be obtained from reference 24 as

$$\mu_{H_2} = (0.66 \times 10^{-6})(T)^{3/2}/(T + 70.5) \tag{5.8}$$

$$\mu_{He} = (1.55 \times 10^{-6})(T)^{3/2}/(T + 97.8) \tag{5.9}$$

The thermal conductivity of H_2 and H are obtained from reference 25 as

$$K_{H_2} = 3.212 \times 10^{-5} + (5.344 \times 10^{-8})T \tag{5.10}$$

$$K_H = 2.496 \times 10^{-5} + (5.129 \times 10^{-8})T \tag{5.11}$$

The viscosity of H and thermal conductivity of He are obtained from the relation between viscosity and thermal conductivity of monatomic gases as given in reference 23 by

$$K = (15/4)(R/M)\mu \tag{5.12}$$

Very little information is available on transport properties of other species such as H_2^+, H^+, e^-, etc. Fortunately, transport properties are important only in the boundary-layer region where the temperature is not high enough to produce these species.

It should be noted that all relations presented in this section are expressed in dimensional form; hence, use of asterisks as superscripts on dimensional quantities has been left out for convenience.

6. EQUILIBRIUM CHEMICAL COMPOSITION

Analyses of chemically reacting flows are usually simplified by assuming the chemical equilibrium behavior of the gas mixture. In this section, information on chemical equilibrium reactions and reaction rates are provided for the shock-layer gas mixture of a Jovian entry body.

For chemical equilibrium composition of the shock-layer gas, a computer code developed by Sutton (ref. 26) is used in this study. The number density of eight chemical species, H_2, H, H^+, H^-, e^-, He, He^+, He^{++} are calculated by the five following chemical reactions.

1. $H_2 \rightleftarrows 2H$
2. $H \rightleftarrows H^+ + e^-$
3. $He \rightleftarrows He^+ + e^-$
4. $He^+ \rightleftarrows He^{++} + e^-$
5. $H^- \rightleftarrows H + e^-$

In general, these reactions can be expressed by

$$\sum a_i A_i \rightleftarrows \sum b_i B_i \tag{6.1}$$

The number density of particles (particle/m^3) is related to the equilibrium rate constant and can be expressed as (ref 27).

$$K_j = [\Pi N^{b_i}(B_i)]/[\Pi N^{a_i}(A_i)] \tag{6.2}$$

Form the species partition function, the equilibrium rate constants for the five reactions are

$$\left.\begin{aligned}
\ln K_1 &= 66.02 + 0.5 \ln T + \ln[1 - \exp(-6331/T)] - 51964/T \\
\ln K_2 &= 49.24 + 1.5 \ln T - 157810/T \\
\ln K_3 &= 50.63 + 1.5 \ln T - 285287/T \\
\ln K_4 &= 49.24 + 1.5 \ln T - 631310/T \\
\ln K_5 &= 50.63 + 1.5 \ln T - 8750/T
\end{aligned}\right\} \tag{6.3}$$

The chemical reactions and reaction rates are listed in table 2.

The conservation equations for hydrogen and helium nuclei and charge are

$$N_H + 2N_{H2} + N_{H^+} + N_{H^-} = N_H^o \tag{6.4}$$

$$N_{He} + N_{He^+} + N_{He^{++}} + N_{He}^o \tag{6.5}$$

$$N_{H^+} + N_{He^+} + 2N_{He^{++}} - N_{H^-} = N_{e^-} \tag{6.6}$$

The number densities of the hydrogen and helium nuclei are calculated by

$$N_H^o = 2x_{H_2}(A_o\rho/M_o) \tag{6.7}$$

$$N_{He}^o - x_{He}(A_o\rho/M_o) \tag{6.8}$$

where

$$M_o = 2.016x_{H_2} + 4.003x_{He}$$

In the above equations, A_0 represents Avogadro's constant, ρ is the mixture density in g/cm^3, x_{H_2} is the mole fraction of molecular hydrogen, and x_{He} is the mole fraction of helium.

An approximate solution for the number density is obtained by assuming that the dissociation of molecular hydrogen is essentially completed before ionization of the atomic hydrogen begins, ionization of the hydrogen is completed before the first ionization of helium begins, first ionization of helium is completed before second ionization begins and, finally, the negative ions of hydrogen formed are too small to significantly affect the number of hydrogen atoms and electrons. The solution procedure for obtaining the eight unknown number densities is discussed in reference 26. The closed-form solutions are obtained by solving equation (6.2) for each reaction independently. This is accomplished by setting the appropriate values in equations (6.4) to (6.6) equal to zero if the species are not present in the reaction. The closed-form solutions for the number densities (in particles/cm^3) of each species are given by

$$
\begin{aligned}
H_2: \quad & N_{H_2} + (N_H^O/2) + (K_1/8)\left[(1 + 8N_H^O/K_1)^{1/2} - 1\right] \\
H^+: \quad & N_{H^+} = (K_2/2)\left[(1 + 4N_H^O/K_2)^{1/2} - 1\right] \\
H: \quad & N_H = N_H^O - 2N_{H_2} - N_{H^+} \\
H_e^+: \quad & N_{He^+} = (D_1/2)\left[(1 + 4K_3N_{He}^O/D_1^2)^{1/2} - 1\right], \quad D_1 = K_3 + N_{H^+} \\
He^{++}: \quad & N_{He}^{++} = (D_2/2)\left[(1 + 4K_4N_{He}^O/D_2^2)^{1/2} - 1\right], \quad D_2 = K_4 + N_H + N_{He}^O \\
He: \quad & N_{He} = N_{He}^O - N_{He^+} + N_{He}^{++} \\
e^-: \quad & N_{e^-} = N_{H^+} + N_{He^+} + 2N_{He}^{++} \\
H^-: \quad & N_{H^-} = N_H N_{e^-}/K_5
\end{aligned}
\tag{6.9}
$$

As mentioned earlier, the equilibrium composition of the shock-layer gas is made up of the above eight species.

7. RADIATION MODEL

An appropriate expression for the radiative flux, q_R, is needed for the solution of the energy equation presented in section 3, "Basic Formulation." This requires a suitable transport model and a meaningful spectral model for variation of the absorption coefficient of the gas. In this section, appropriate expressions for the spectral and total radiative flux are given and information on the spectral absorption by the hydrogen/helium gas is presented.

7.1. Radiative Flux Equations

The relation for total radiative flux, in general, is given by (refs. 27 and 28)

$$q_R(x_i) = \int_0^{\infty} \int_0^{4\pi} I_\nu^* e_i \, d\Omega \, d\nu \tag{7.1}$$

where Ω is a solid angle measured in steradians, ν^* is the frequency, I_ν^* is specific intensity and the unit vector in the specific direction for I_ν^* is e_i. The basic equation for the intensity gradient along a ray for a gas in local thermodynamics equilibrium is given by

$$\frac{dI_\nu^*}{ds} = \kappa_\nu^* (B_\nu^* - I_\nu^*) \tag{7.2}$$

where B_ν^* is the Planck function, s is distance, and κ_ν is the linear absorption coefficient corrected for induced emission. The solution of this linear differential equation is found to be

$$I_\nu^* = \int_0^S \kappa_\nu^*(\xi) \, B_\nu^*(\xi) \exp\left[- \int_\xi^S \kappa_\nu^*(\xi') d\xi' \right] d\xi + I_\nu^*(0) \exp\left[- \int_0^S \kappa_\nu^*(\xi) d\xi \right] \tag{7.3}$$

In the present analysis the "tangent slab" assumption for radiative transfer has been used. This implies that the radiative energy transfer along the body is negligible in comparison to that transferred in the direction normal to the body. It should be noted that the tangent slab approximation is used only

for the radiative transport and not for other flow variables. For a non-scattering medium and diffuse nonreflecting bounding surfaces, one-dimensional expression for the spectral radiative flux is given by (refs. 27 and 28)

$$q_{R\nu}(\tau_\nu) = 2\pi\left\{\varepsilon_\nu\left[B_\nu(0)E_3(\tau_\nu) - B_\nu(\tau_{o\nu})E_3(\tau_{o\nu} - \tau_\nu)\right] + \int_0^{\tau_\nu} B_\nu(t)E_2(\tau_\nu - t)dt - \int_{\tau_\nu}^{\tau_{o\nu}} B_\nu(t)E_2(t - \tau_\nu)dt\right\} \tag{7.4}$$

where

$$\tau_\nu = \int_0^y \kappa_\nu(y')dy'$$

$$E_n(t) = \int_0^1 \exp(-t/\mu)\mu^{n-2}\, d\mu$$

$$B_\nu = (h\nu^3/c^2)/[\exp(h\nu/kT) - 1]$$

The quantities $B_\nu(0)$ and $B_\nu(\tau_{o\nu})$ represent the radiosities of the body surface and shock respectively.

The expression of total radiative flux is given by

$$q_R = \int_0^\infty q_{R\nu}(\tau_\nu)d\nu \tag{7.5}$$

In the shock layer, the radiative energy from the bow shock usually is neglected in comparison to the energy absorbed and emitted by the gas layer. The expression for net radiative flux in the shock layer, therefore, is given by

$$q_R = 2\int_0^\infty \left\{q_\nu(0)E_3(\tau_\nu) + \pi\left[\int_0^{\tau_\nu} B_\nu(t)E_2(\tau_\nu - t)dt - \int_{\tau_\nu}^{\tau_{o\nu}} B_\nu(t)E_2(t - \tau_\nu)dt\right]\right\}d\nu \tag{7.6a}$$

where

$$q_\nu(0) = \varepsilon_\nu \pi B_\nu(T_w)$$

In this equation, the first two terms on the right represent the radiative energy transfer towards the bow shock while the third term represents the energy transfer towards the body. Upon denoting these contributions by q_R^+ and q_R^-, equation (7.6a) can be written as

$$q_R = q_R^+ + q_R^- \tag{7.6b}$$

A few spectral models for absorption by the hydrogen-helium species in the shock layer have been proposed in the literature (refs. 26,29,30). For Jovian entry conditions, the absorption by helium usually is neglected. The spectral absorption of hydrogen species was represented by a 58-step model by Sutton (ref. 26) and was approximated by a 30-step model by Tiwari and Subramanian (ref. 30). The results of these step models are compared with the detailed model of Nicolet (ref. 29). The 58-step model proposed by Sutton is employed in this study. The details of radiative absorption by the 58-step model are available in reference 26, and these are summarized in the next subsection. In essence, the step model replaces the frequency integration in equation (7.6) by a summation over 58 different frequency intervals. In each frequency interval, the absorption coefficient is taken to be constant. For this model, equation (7.6) can be expressed as

$$\begin{aligned} q_R = 2\pi \sum_{j=1}^{N} \Bigg\{ & \varepsilon_\nu B_\nu(T_w) E_3\left[\int_0^y \kappa_\nu(y')dy'\right] \\ & + \int_0^y \kappa_\nu(\xi) B_\nu(\xi) E_2\left[\int_\xi^y \kappa_\nu(y')dy'\right] d\xi \\ & - \int_y^{y_s} \kappa_\nu(\xi) B_\nu(\xi) E_2\left[\int_y^\xi \kappa_\nu(y')dy'\right] d\xi \Bigg\} \end{aligned} \tag{7.7}$$

where y_s denotes the shock location and N is the number of spectral intervals In each of the ith intervals, the absorption coefficient, but not the Planck function, is assumed constant. In accordance with equation (7.6b), equation (7.7) can be expressed in terms of q_R^+ and q_R^-, and for a gray body one finds

$$\begin{aligned} q_R^+(y) = (4\pi h/c^2) \sum_{j=1}^{N} \Bigg\{ & \varepsilon F(\nu_j, T_w) E_3\left[\int_0^y \kappa_{\nu j}(y')dy'\right] \\ & + \int_0^y (kT/h)^4 F(\nu_j, T) \kappa_{\nu j}(\xi) E_2\left[\int_\xi^y \kappa_{\nu j}(y')dy'\right] d\xi \Bigg\} \end{aligned} \tag{7.8a}$$

$$q_R^-(y) = -(4\pi h/c^2)\sum_{j=1}^{N}\left\{\int_y^{y_s}(kT/h)^4 F(\nu_j,T)\kappa_{\nu j}E_2\left[\int_y^{\xi}\kappa_{\nu j}(y')dy'\right]d\xi\right\} \tag{7.8b}$$

7.2. Absorption Model

As mentioned earlier, the 58-step model proposed by Sutton (ref. 26) for spectral absorption by the hydrogen species in the shock layer is employed in this study. For atomic hydrogen, all three transitions (bound-bound, bound-free, and free-free) are considered. The total absorption of the ith step is a summation of the average absorption for the ith transitions in the jth step, i.e.

$$\bar{\kappa}_j = \sum_i \kappa_{ij} \tag{7.9a}$$

$$\kappa_{ij} = (1/\Delta\nu_j)\int_{\nu_j}^{\nu_j+\Delta\nu_j}\kappa_i d\nu \tag{7.9b}$$

$$\kappa_i = f(T,N_i,\nu) \tag{7.9c}$$

where N_i represents the number density in cm^{-3}.

For the free-free transition, the absorption coefficient is calculated by

$$\kappa_{ff}^H = (2.61E - 35)N_e H_{H^+}/\nu^3 T^{\frac{1}{2}}) \tag{7.10}$$

The absorption coefficient for bound-free transitons is calculated by employing two separate relations as

$$\kappa_{bf}^H = (1.99E - 14)(N_H/\nu^3)\sum_{n_\ell=1}^{4}(1/n_\ell^3)\exp(C_1),\ 1 \le n_\ell \le 4 \tag{7.11a}$$

$$\kappa_{bf}^H = (6.31E - 20)(TN_H/\nu^3)\exp(C_2)\exp(C_3),\ 5 \le n_\ell \le n_{\ell,max} \tag{7.11b}$$

where

$$C_1 = (-157780/T)[1 - (1/n_\ell^2)]$$

$$C_2 = (-157780/T)(1 - \delta/13.6)$$

$$C_3 = [(157780/T)(1/25 - \delta/13.6)] - 1$$

$$\delta = (1.79E - 5)\left(N_e^{2/7}\right)/\left(T^{1/7}\right)$$

In the above equations, n_ℓ represents the principal quantum numbers, δ is the reduction in ionization potential in eV, and the values 157780 and 13.6 are the ionization potential in K and eV respectively.

The bound-bound transitions are included for principle quantum numbers up to five. The absorption coefficient is calculated by using the relation

$$\kappa_{bb}^{H} = SL(\nu) \qquad (7.12)$$

where S is the line strength and $L(\nu)$ is the line shape factor. The line strength is given by the relation

$$S = (1.10E - 16) f n_\ell^2 N_H \exp[(-157780/T)(1 - 1/n_\ell^2)] \qquad (7.13)$$

The line shape factor is given by the relation

$$L(\nu) = \gamma/\{\pi[\gamma^2 + (\nu - \nu_o)^2]\} \qquad (7.14)$$

where ν_o is the frequency at the line center and γ is the line half width and these are given by

$$\nu_o = 13.6\left[(1/n_\ell^2) - (1/n_u^2)\right] \qquad (7.15)$$

$$\gamma = a\left[1.05E\ 15(n_u^2 - n_\ell^2)N_e^{2/3}\right] \qquad (7.16)$$

The constant a in the above equation is taken to be 0.642 for the first line and unity for the remaining lines.

The absorption coefficients for the free-free and bound-free transitions of the negative hydrogen are

$$\kappa_{ff}^{H^-} = (6.02E - 39)N_H N_e/\nu^3 \tag{7.17}$$

$$\kappa_{bf}^{H^-} = (2.89E - 17)(\beta^4 - 4\beta^3 + 3.64\beta^2 + 0.73\beta)N_{H^-} \tag{7.18}$$

where $\beta = 1.502/\nu$. The threshold for the bound-free transition of H^- is 0.757 eV.

The absorption coefficient for molecular hydrogen in the jth step is obtained in accordance with equation (7.9) and is expressed as

$$\bar{\kappa}_j^{H_2} = f_j(T)N_{H_2} \tag{7.19}$$

where $f_j(T)$ is dependent on the particular step. The molecular bands cover the steps from 7 to 17 eV.

Further details on constructing the step-function model and utilizing it in the radiative flux equations are given in references 24 to 26.

8. METHOD OF SOLUTION

A numerical procedure for solving the viscous shock-layer equations for stagnation and downstream regions is given by Davis (ref. 11). Moss applied this method of solution to reacting multicomponent mixtures in reference 12. A modified form of this procedure is used in this study to obtain solutions of the viscous shock-layer equations. In this method, a transformation is applied to the viscous shock-layer equations in order to simplify the numerical computations. In this transformation most of the variables are normalized with their local shock values. The transformed variables are (ref. 12)

$$\begin{aligned}
\eta &= y/y_s & \bar{p} &= p/p_s & \bar{\mu} &= \mu/\mu_s \\
\xi &= x & \bar{\rho} &= \rho/\rho_s & \bar{K} &= K/K_s \\
\bar{u} &= u/u_s & \bar{T} &= T/T_s & \bar{C}_p &= C_p/C_{ps} \\
\bar{v} &= v/v_s & \bar{H} &= H/H_s
\end{aligned} \tag{8.1}$$

The transformations relating the differential quantities are

$$\frac{\partial(\ )}{\partial x} = \frac{\partial(\ )}{\partial \xi} - \frac{\eta}{y_s}\frac{dy_s}{d\xi}\frac{\partial(\ )}{\partial \eta} \tag{8.2}$$

$$\frac{\partial(\ )}{\partial y} = \frac{1}{y_s}\frac{\partial(\ )}{\partial \eta} \tag{8.3}$$

$$\frac{\partial^2(\ )}{\partial y^2} = \frac{1}{y_s^2}\frac{\partial^2(\ )}{\partial \eta} \tag{8.4}$$

The new form of x-momentum and energy equations in the ξ,η plane can be written as

$$\frac{\partial^2 W}{\partial \eta^2} + C_1\frac{\partial W}{\partial \eta} + C_2 W + C_3 + C_4\frac{\partial W}{\partial \xi} \tag{8.5}$$

where W equals $\bar{u}$ and $\bar{T}$ in the x-momentum and energy equations respectively. The coefficients C_1 and C_4 are given by Moss (ref. 12). Other governing equations are expressed as

Continuity:

$$\frac{\partial}{\partial \xi}\left[y_s(r + y_s\,\eta\cos\theta)\rho_s u_s \bar{\rho}\bar{u}\right] + \frac{\partial}{\partial \eta}\left\{(r + y_s\,\eta\cos\theta)\right.$$

$$\left.\left[(1 + \eta\, y_s\,\kappa)\,\rho_s v_s \bar{\rho}\bar{v} - y_s'\,\eta\,\rho_s\,u_s\,\bar{\rho}\bar{u}\right]\right\} = 0 \tag{8.6}$$

n-momentum

$$\frac{\bar{\rho}\bar{u}}{1 + y_s\eta\kappa}\left[\frac{\partial v_s/\partial \xi}{v_s}\bar{v} + \frac{\partial \bar{v}}{\partial \xi} - (\partial y_s/\partial \xi)(\eta/n_s)(\partial \bar{v}/\partial \eta)\right] + \frac{v_s\bar{\rho}\bar{v}}{u_s y_s}\frac{\partial \bar{v}}{\partial \eta}$$

$$- \frac{u_s}{v_s}\frac{\kappa}{1 + y_s\eta\kappa}\bar{\rho}\bar{u}^2 + \frac{p_s}{\rho_s u_s y_s v_s}\left(\frac{\partial \bar{p}}{\partial \eta}\right) = 0 \tag{8.7a}$$

If thin shock layer is assumed, then the above equation reduces to

$$\frac{\partial p}{\partial \eta} = \frac{\rho_s u_s^2}{p_s(1 + y_s \eta \kappa)} \bar{\rho}\bar{u}^2 \tag{8.7b}$$

The finite-difference scheme used to solve the equation is an implicit method with a forward difference in $\partial w/\partial \xi$ at point (m,n). The shock layer is considered as a network of nodal points with a variable grid spacing in the n direction. The scheme is shown in the figure 2 where m is a station measured along the body surface and n denotes the station measured normal to the body surface. A difference equation is obtained by employing Taylor series expansion into differential equations (7.5) to (7.7) as

$$A_n W_{m,n+1} + B_n W_{m,n} + C_n W_{m,n-1} + D_n = 0 \tag{8.8}$$

where

$$A_n = (2 + C_1 \Delta\eta_{n-1})/[\Delta\eta_n(\Delta\eta_n + \Delta\eta_{n-1})]$$

$$B_n = -[2 - C_1(\Delta\eta_n - \Delta\eta_{n-1})]/(\Delta\eta_n \Delta\eta_{n-1}) - C_2 - C_4/\Delta\xi_{m-1}$$

$$C_n = (2 - C_1 \Delta\eta_n)/[\Delta\eta_{n-1}(\Delta\eta_n + \Delta\eta_{n-1})]$$

$$D_n = C_3 - C_4 W_{m-1,n}/\Delta\xi_{m-1}$$

If it is assumed that

$$W_{m,n} = E_n W_{m,n+1} + F_n \tag{8.9}$$

then equation (7.8) can be written as

$$W_{m,n} = [-A_n/(B_n + C_n E_{n-1})] W_{m,n+1} + (-D_1 - C_n F_{n-1})/(B_n + C_n E_{n-1}) \tag{8.10}$$

$$E_n = -A_n/(B_n + C_n E_{n-1}) \tag{8.11}$$

$$F_n = (-D_n - C_n F_{n-1})/(B_n + C_n E_{n-1}) \tag{8.12}$$

Since E_1 and E_2 are known from the boundary conditions, E_n and F_n can be calculated from equations (7.11) and (7.12). The quantities at point m,n are obtained from equation (7.9).

The procedure for solution is to start solving the modified Rankine-Hugoniot equations to obtain the properties immediately behind the shock by using free-stream conditions and assuming $\partial N_s/\partial \xi = 0$. With the shock and body surface conditions know, the properties in the shock layer can be calculated. The first pass is only an approximate solution because the thin-layer form is used in the n-momentum equation, and the shock wave angle equal to the body angle is assumed. All these assumptions are removed by iteration in the next pass. The discussion of the solution procedure, in detail, can be found in references 12 and 14.

9. RESULTS AND DISCUSSION

The governing equations of the shock-layer region with body- and shock-slip boundary conditions were solved for a physically realistic Jovian entry condition (see table 3). Because the chemical equilibrium is assumed and thickness effect is of higher order, the concentration slip and thickness effects were neglected in this study. The solutions were obtained for flow past a 45-degree hyperboloid at an angle of attack of zero degree. An atmospheric model that consists of 85 percent H_2 and 15 percent He (by mole fraction) was used. The surface temperature of the entry body was assumed to be 4,000 K, and the nose radius is taken to be 23 cm in all cases.

By invoking the body and shock-slip conditions, results for variation in the shock-layer flow properties were calculated for higher altitude entry conditions. Some important results of this investigation are presented in this section. Results are presented first for the velocity and temperature jumps at the body surface. Following this, results are presented for the properties immediately behind the shock. Next, the effects of radiation on convective heating at higher altitudes are discussed. Finally, to assess the influence of slip conditions, results are presented for the convective and radiative heating. It should be emphasized here that the term "slip conditions" (or "slip boundary conditions"), as used in this study, implies both the body- and the shock-slip conditions.

The variation in the surface-slip velocity is illustrated in figure 3 as a function of the entry altitude. Since u-velocity was almost zero at the stagnation streamline, the results presented in figure 3 have been obtained for location (or station) 3 of figure 2. Figure 3 clearly illustrates that the condition of no slip was not satisfied at higher altitudes. Since $\bar{u}$ was normalized by the shock value (i.e., $\bar{u} = u/u_s$), the magnitude of velocity slip can be expressed as a percent of u_s. It is evident from figure 3 that about 8 percent velocity slip occured at Z = 261 km and only 0.1 percent at Z = 143 km.

The temperature jump at the body surface is shown in figure 4 for different entry altitudes. The results presented in this figure are for the case with no radiation; in obtaining these results, the body surface temperature was taken to be 4,000 K. A temperature jump of about 18 percent (i.e., ∇T = 680 K) was noted at the stagnation point for entry conditions at Z = 261 km. At lower altitudes, however, the temperature jump was seen to be relatively small. For example, at Z = 116 km, the temperature jump is only 3 K.

Figures 5 to 7 show the temperature jump, velocity slip, density and total enthalpy changes just behind the shock. It is evident from figure 5 that when the altitude was lower than 225 km, the shock slip conditions were not important. However, a significant temperature difference was noted at Z = 261 km. The results presented in figure 6 illustrate that both the u and v velocity components were influenced by the slip conditions. Since both the temperature and velocity components decreased just behind the shock, the slip conditions resulted in an increase in density and a decrease in total enthalpy. This is clearly evident from the results of figure 7.

Figure 8 shows how the convective heat flux was affected by radiation. The results indicate that at low altitudes the convective heat flux decreased with increasing altitude and at high altitudes it increased with altitude. This is because at different ranges of altitude, the temperature distribution was rearranged by the radiation effects. It is noted that a maximum of 50 percent change in convective heat transfer occurred at Z = 261 km and a 25 percent change at Z = 225 km.

Figure 9 shows how the radiative heat flux was affected by slip boundary conditions. It is seen that the effect was very small at altitudes lower than

225 km. It was found that there was approximately 50 percent reduction in radiative heat flux due to the shock temperature jump at 261 km.

The effects of slip boundary conditions on convective heat flux toward the body (along the body surface) are illustrated in figures 10 and 11, for the cases with and without the radiation interaction. The results indicate that the slip conditions started to effect the convective heat flux at Z = 225 km (ε = 0.09064) by approximately 8 percent (at stagnation point), and this increased to 27 percent at Z = 261 km (ε = 0.2129). The effect was seen to increase with the distance away from the stagnation point, and inclusion of radiation was seen to suppress this influence. When the altitude was less than 225 km, the effect of slip boundary conditions was relatively small and could be neglected.

10. CONCLUSIONS

Results of this study indicate that the slip boundary conditions (both at the shock wave and the body) should be employed in investigating the flow phenomena around a Jovian entry when entry altitudes are higher than 225 km. The convective heat flux is influenced more greatly by the body-slip conditions than by the shock-slip conditions. The radiative flux, however, is affected largely by the shock-slip conditions. Although the extent of radiative contribution is small at higher altitudes, the radiative heat flux term should not be neglected from the energy equation because it has a significant influence on the convective heat flux. For further study, it is suggested that the shock-slip conditions be investigated by considering the thickness effect; also the influence of concentration-slip should be included. Furthermore, it would be advisable to separate the shock- and surface-slip conditions and investigate their influences separately.

REFERENCES

1. Hayes, W.D.; and Probstein, R.F.: Hypersonic Flow Theory. Academic Press, 1959 and 1966.

2. Probstein, F.F.: Shock-Wave and Flow Field Development in Hypersonic Reentry. ARS J., Vol. 31, 1961, pp. 185-194.

3. Cheng, H.K.: The Blunt-Body Problem in Hypersonic Flow at Low Reynolds-Number. Inst. Aerospace Science Paper No. 63-92, 1963.

4. Rott, N.; and Lenard, M.: The Effect of Slip, Particularly for Highly Cooled Wall. J. Aerosp. Sci., Vol. 29, 1962, pp. 591-595.

5. Probstein, R.F.; and Pan, Y.S.: Shock Structure and Leading Edge Problem. In: Rarefied Gas Dynamics, Vol. 2, J.A. Laurmann, ed., Academic Press (NY), 1963.

6. Pan; Y.S.; and Probstein, R.F.: Rarefied-Flow Transition at a Leading Edge. In: Foundamental Phenomena in Hypersonic Flow, J.G. Hall, ed., Cornell University Press, 1966.

7. Shidlovsky, V.P.: Introduction to Rarefied Gases. American Elsevier Publishing Company Inc. (NY), 1967.

8. Kogan, M.N.: Rarefied Gas Dynamics. Plenum (NY), 1969, pp. 367-400.

9. Scott, C.D.: Reacting Shock Layer with Slip and Catalytic Boundary Condition. AIAA, Vol. 13, Oct. 1975, pp. 1271-1278.

10. Walberg, G.D.; Jones, J.J.; Olstad, W.B.; Sutton, K.; Moss, J.N.; and Powell, R.W.: An Investigation of the Effects of Mass Loss Shape Change and Real Gas Aerodynamics on a Jovian Atmospheric Reconstruction Experiment. Paper No. 76-073, presented at the XXVIIth Congress of the International Astronautical Federation, Oct. 10-16, 1976.

11. Davis, R.T.: Numerical Solution of the Hypersonic Viscous Shock-Layer Equations. AIAA, Vol. 8, No. 5, May 1970, pp. 843-851; also, Hypersonic Flow of a Chemically Reacting Binary Mixture Past a Blunt Body. AIAA Paper No. 70-805, July 1970.

12. Moss, J.N.: Reacting Viscous-Shock-Layer Solutions with Multicomponent Diffusion and Mass Injection. NASA TR R-411, June 1974.

13. Moss, J.N.; Anderson, E.C.; and Bolz, C.W.: Aerothermal Environment for Jovian Entry. AIAA Paper No. 76-469, July 1976.

14. Tiwari, S.N.; and Szema, K.Y.: Influence of Precursor Heating on Viscous Flow Around a Jovian Entry Body. AIAA Paper No. 78-190, Jan. 1978; also, NASA TR NAS1-14193-27, Sept. 1978.

15. Zoby, E.V.; Gnoffo, P.A.; and Graves, R.A.: Correlation for Determining Thermodynamic Properties of Hydrogen-Helium Gas Mixtures at Temperatures from 7000 to 35000 K. NASA TN D-8262, Aug. 1976.

16. Street, R.E.: Problem of Slip Flow in Aerodynamics. NASA RM S-7A30, 1957; also, A Study of Boundary Conduction in Slip-Flow Aerodynamics. In: Rarefied Gas Dynamics, F.M. Devienne, ed., London Pergamon Press, 1960, pp. 276-292.

17. Davis, R.T.; and Flügge-Lotz, I. Second Order Boundary-Layer Effect in Hypersonic Flow Past Axisymmetric Blunt Bodies. J. Fluid Mech., Vol. 20, May 1964, pp. 593-623.

18. Probstein, R.F.; and Kemp, H.N.: J. Aerosp. Sci., Vol. 27, 1960, pp. 174-193.

19. Chow, R.R.; and Ting, L.: J. Aerosp. Sci., Vol. 28, 1961, pp. 428-430.

20. Van Dyke, M.D.: Perturbation Method in Fluid Mechanics. Academic Press (NY), 1964.

21. McBride, B.J.; Hermel, S.: Ehlers, J.G.; and Gordon, S.: Thermodynamic Properties to 6000°K for 210 Substances Involving the First 18 Elements. NASA Report, SP-3001, 1963.

22. Babu, S.G.: Approximate Thermochemical Tables for Some C-H and C-H-O Species. NASA CR-2187, Mar. 1973.

23. Bird, R.B.; Stewart, W.E.; and Lightfoot, E.N.: Transport Phenomena. John Wiley & Sons, Inc., 1960.

24. Hall, N.A.: Thermodynamics Fluid Flow. Prentice Hall, Inc., 1957.

25. Esch, D.D.; Pike, R.W.; Engel, C.D.; Farmer, R.C.; and Balhoff, J.F.: Stagnation Region Heating of a Phenotic-Nylon Ablator During Return from Planetary Mission. NASA CR-112026, Sept. 1971.

Inviscid Radiation Flow Field Analysis of Outer Planet Entry Probes. AIAA Paper No. 78-189, Jan. 1978.

27. Vincenti, W.G.; and Kruger, C.H.: Introduction to Physical Dynamics. John Wiley and Sons, Inc., 1965.

28. Sparrow, E.M.; and Cess, R.D.: Radiation Heat Transfer. Brooks/Cole Publishing Co. (Belmont, CA), 1966.

29. Nicolet, W.E.: Users Manual for RAD/EQUIL/, 1973, A General Purpose Radiation Transport Program. NASA CR-132470, 1973.

30. Tiwari, S.N.; and Subramanian, S.V.: Significance of Radiation Models in Investigating the Flow Phenomena Around a Jovian Entry Body. AIAA Paper No. 78-188, Jan. 1978; also, NASA TR NAS1-14193-26, Oct. 1978.

Table 1. Coefficient for evaluation of the specific heat at constant pressure and enthalpy for various hydrogen/helium species.

Species	Coefficients						Temp. Range °K
	a_1	a_2	a_3	a_4	a_5	a_6	
	2.5	0	0	0	0	2.547162E+4	> 300
H	2.5	0	0	0	0	2.547162E+4	> 1,000
	2.475164	7.366387E-5	-2.537593E-8	2.386674E-12	4.551431E-17	2.523626E+4	> 6,000
	3.057445	2.676520E-3	-5.809916E-6	5.521039E-9	-1.812273E-12	-9.889047E+2	> 300
H_2	3.10019	5.111946E-4	5.264421E-8	-3.490997E-11	3.694534E-15	-8.773804E+2	> 1,000
	3.363	4.656000E-4	-5.127000E-8	2.802000E-12	4.905000E-17	-1.018000E+3	> 6,000
	2.5	0	0	0	0	1.840334E+5	> 300
H^+	2.5	0	0	0	0	1.840334E+5	> 1,000
	2.5	0	0	0	0	1.840334E+5	> 6,000
	2.5	0	0	0	0	-7.453749E+2	> 300
He	2.5	0	0	0	0	-7.453749E+2	> 1,000
	2.5	0	0	0	0	-7.453749E+2	> 6,000
	2.5	0	0	0	0	2.853426E+5	> 300
He^+	2.5	0	0	0	0	2.853426E+5	> 1,000
	2.5	0	0	0	0	2.853426E+5	> 6,000
	2.5	0	0	0	0	-7.453749E+2	> 300
e^-	2.5	0	0	0	0	-7.453749E+2	> 1,000
	2.508	-6.332000E-6	1.364000E-9	-1.094000E-13	2.934000E-18	-7.450000E+2	> 6,000

Table 2. Equilibrium reaction scheme and rate constants.

	Reactions	Rate Constants	Particles/m^3
1.	$H_2 \rightleftarrows 2H$	$k_1 = 4.699E22\ T^{\frac{1}{2}}$	$(1-\exp(-6331/T)\ \exp(-51964/T)$
2.	$H \rightleftarrows H^+ + e^-$	$k_2 = 2.411E15\ T^{1.5}$	$\exp(-157819/T)$
3.	$He \rightleftarrows He^+ + e^-$	$k_3 = 9.645E15\ T^{1.5}$	$\exp(-285287/T)$
4.	$H_e + \rightleftarrows He^{++} + e^-$	$k_4 = 2.411E15\ T^{1.5}$	$\exp(-631310/T)$
5.	$H^- \rightleftarrows H^+e^-$	$k_5 = 9.643E15\ T^{1.5}$	$\exp(-8750/T)$

Table 5. Altitudes and free-stream Jupiter entry conditions.

Z	$\bar{V}_\infty$	ρ_∞	T_∞	p_∞	$\rho_\infty \bar{V}_\infty^3$	ε
km	cm/sec	g/cm^3	°K	$dyne/cm^2$		
116	3.909E6	4.65E-7	145	2.44E3	2.777E13	0.006645
143	4.517E6	1.27E-7	145	6.66E2	1.17E13	0.01272
190	4.736E6	1.33E-8	145	69	1.412E12	0.03930
225	4.756E6	2.50E-9	145	13	2.69E11	0.09064
261	4.758E6	4.53E-10	145	2.38	4.879E10	0.2129

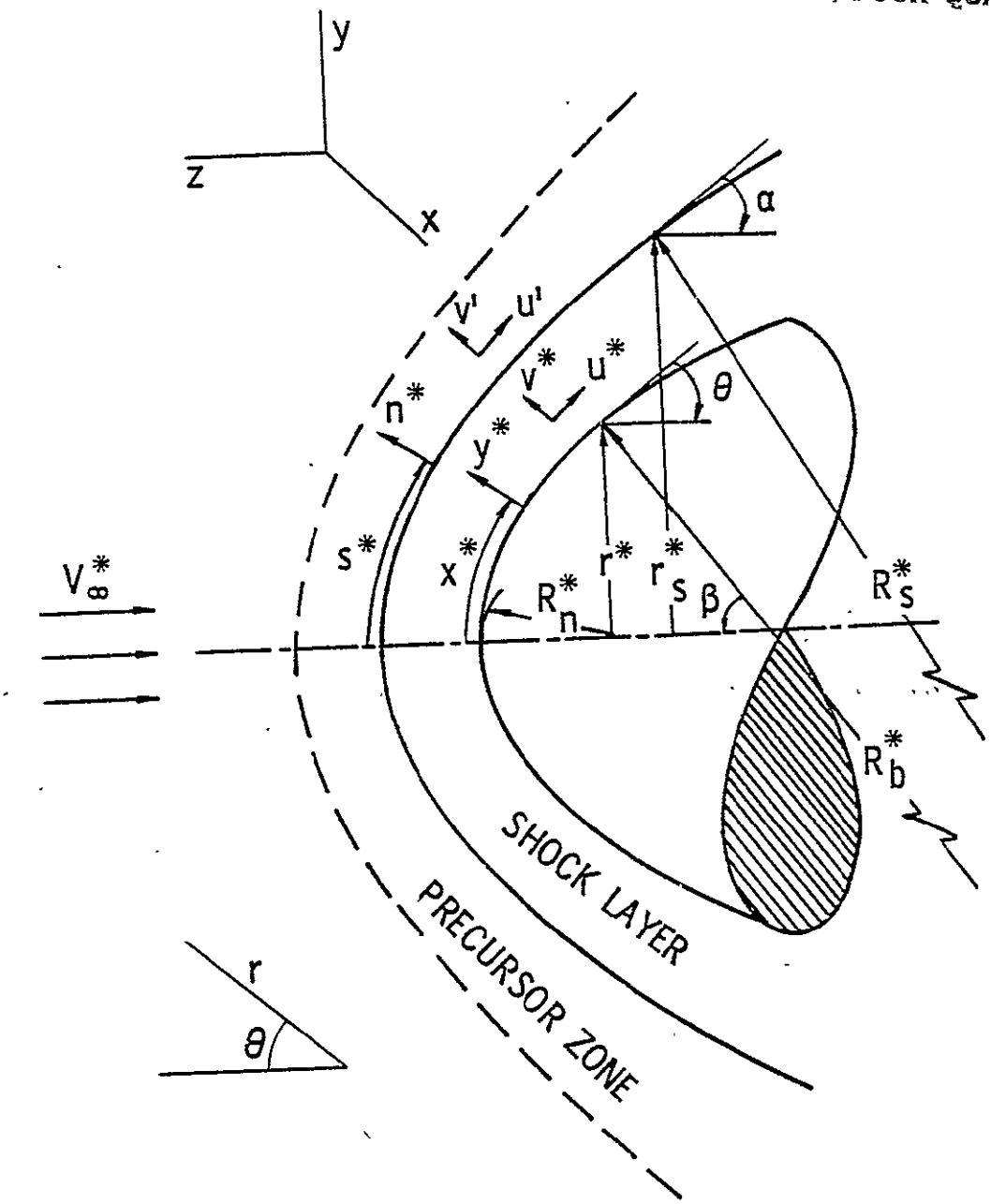

Figure 1. Physical model and coordinate system.

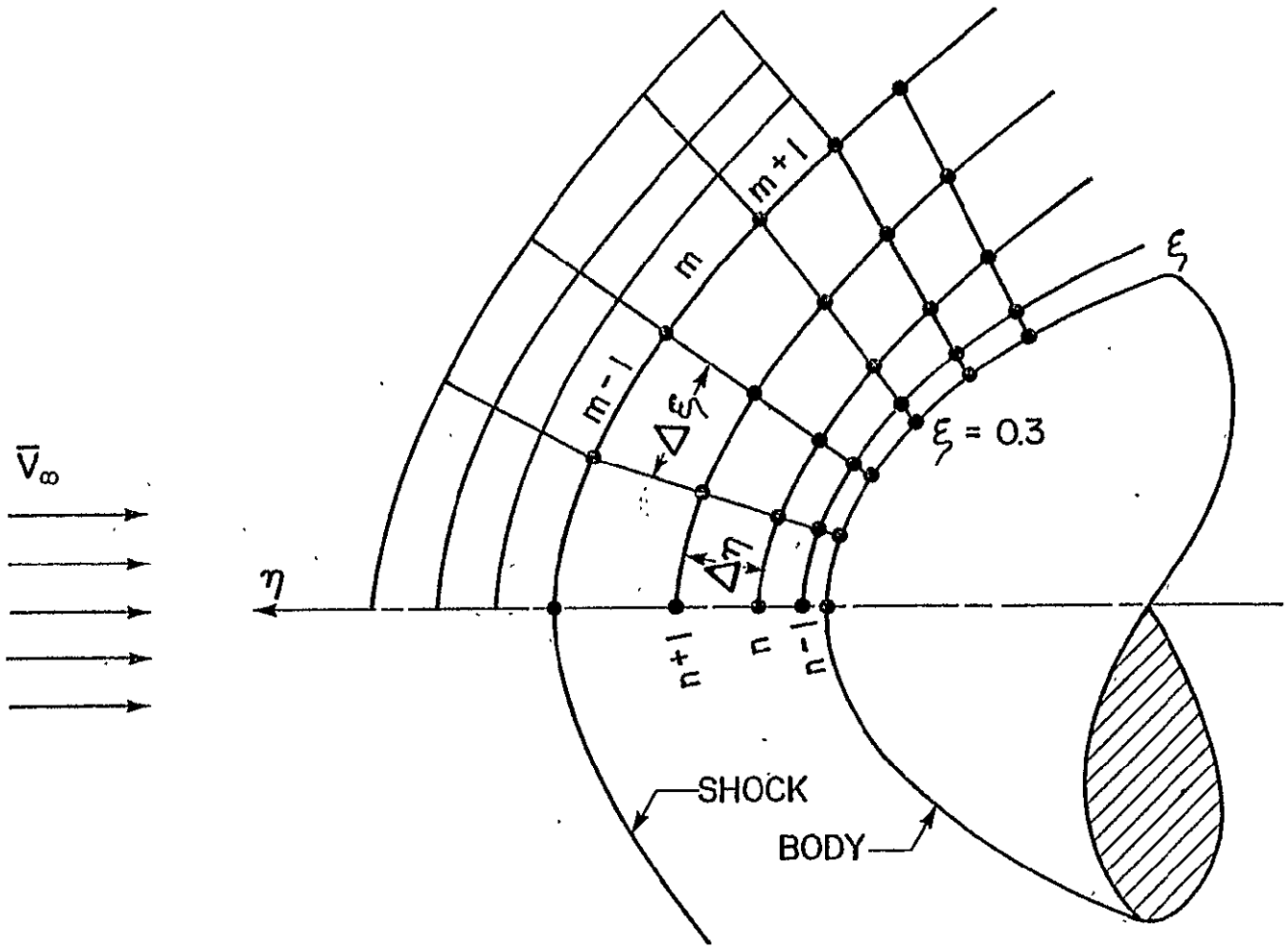

Figure 2. Finite difference representation of flow field.

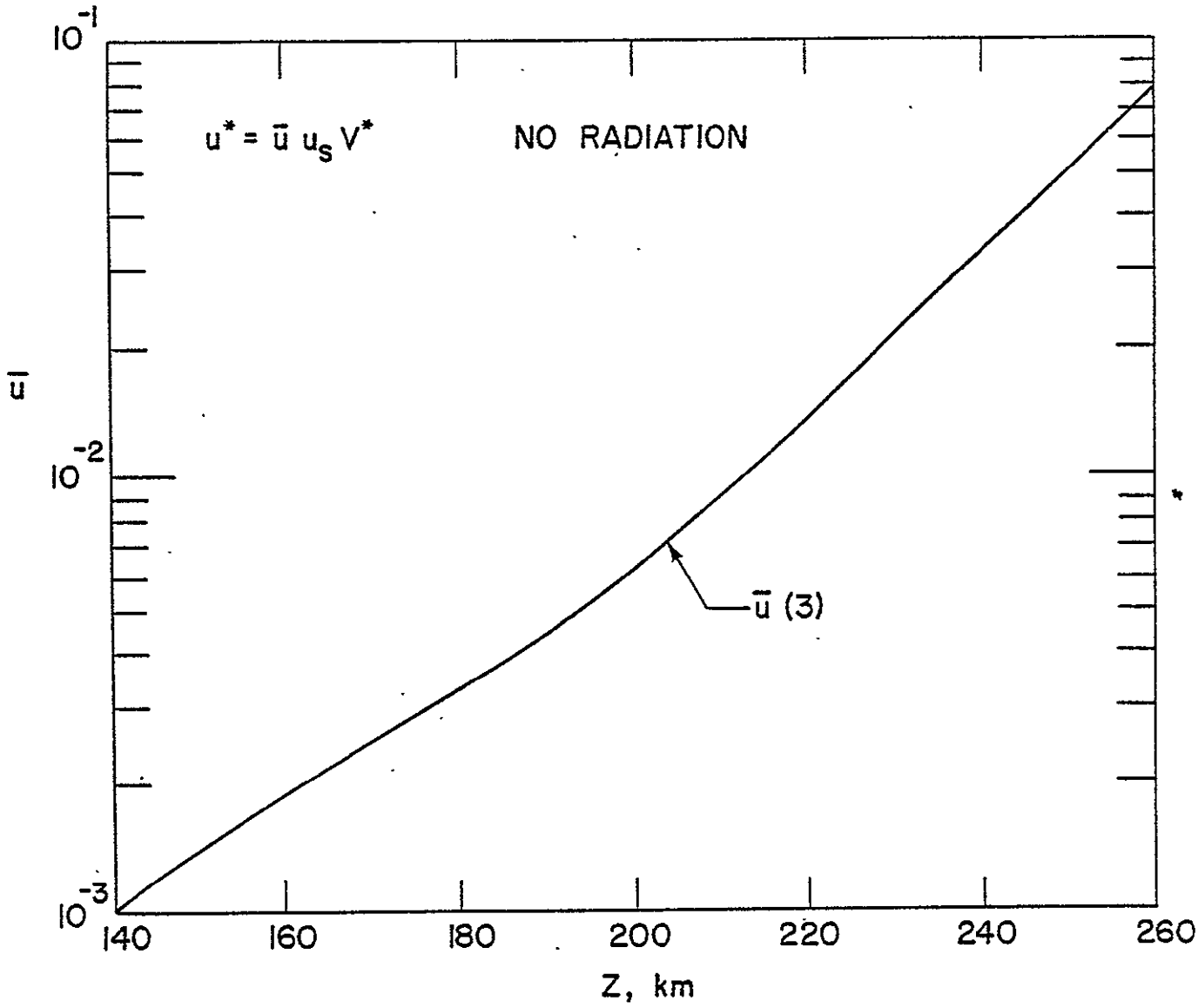

Figure 3. Velocity slip along the body surface.

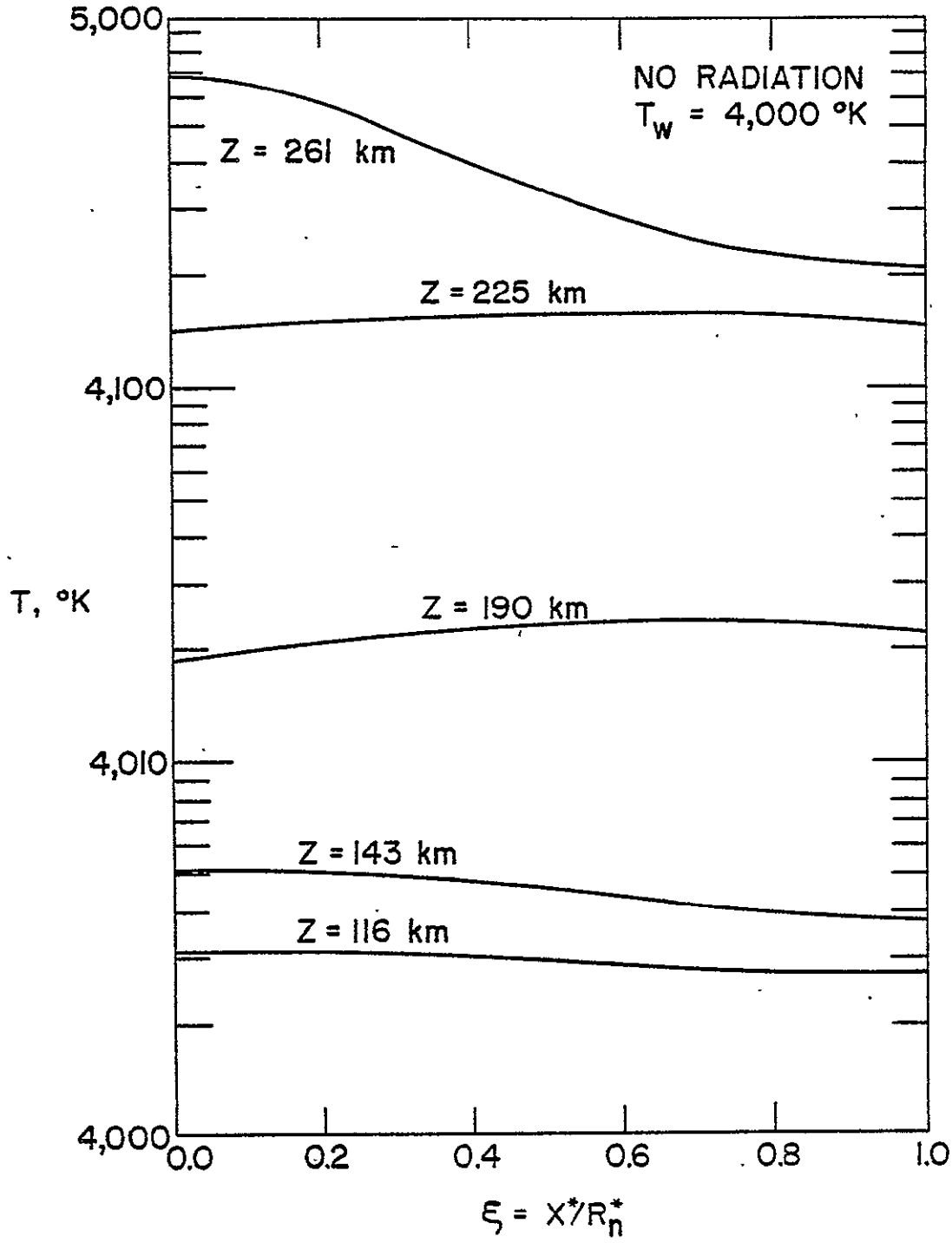

Figure 4. Temperature jump along the body surface for different entry altitudes.

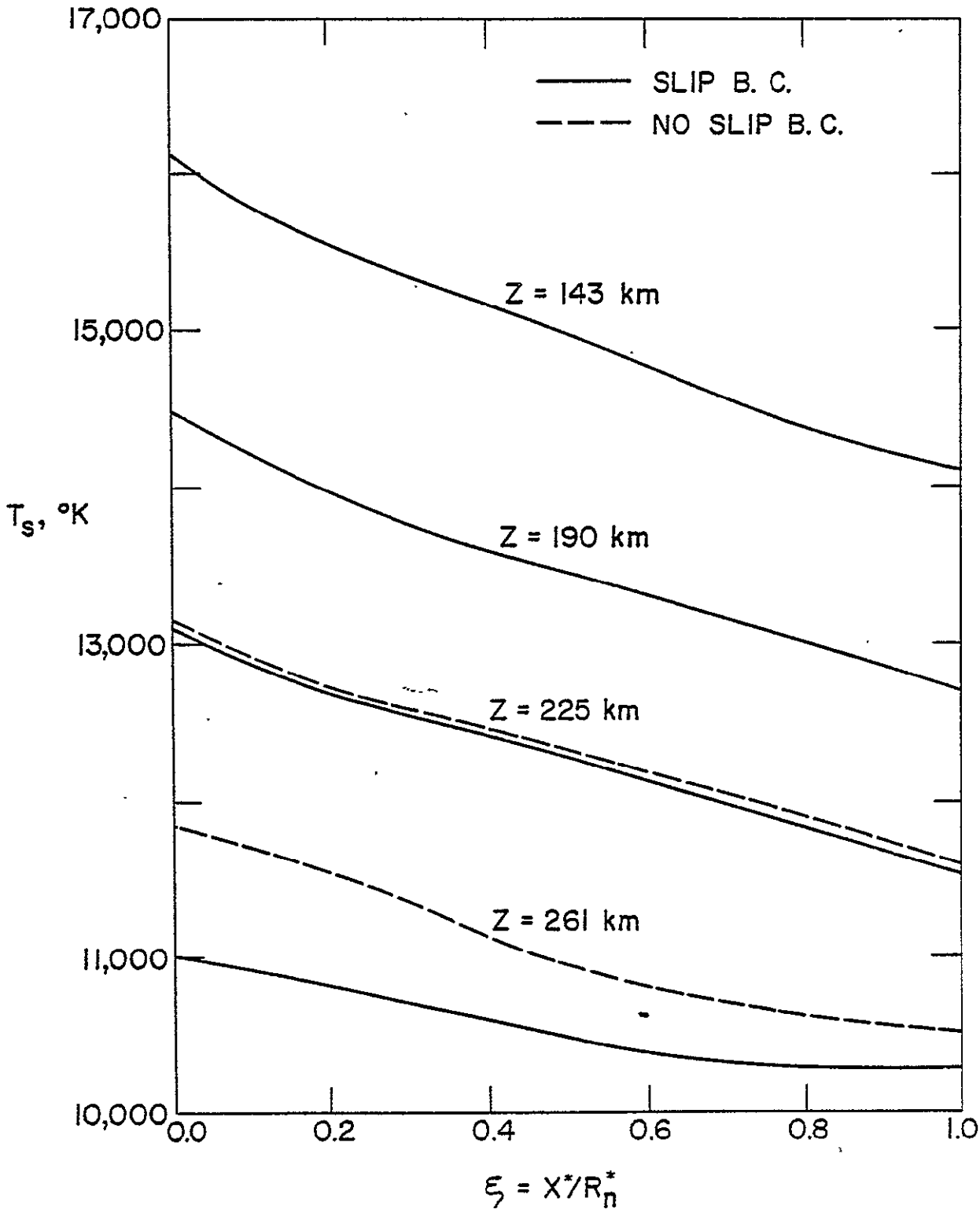

Figure 5. Temperature variation (just behind the shock wave) as a function of ξ-coordinate.

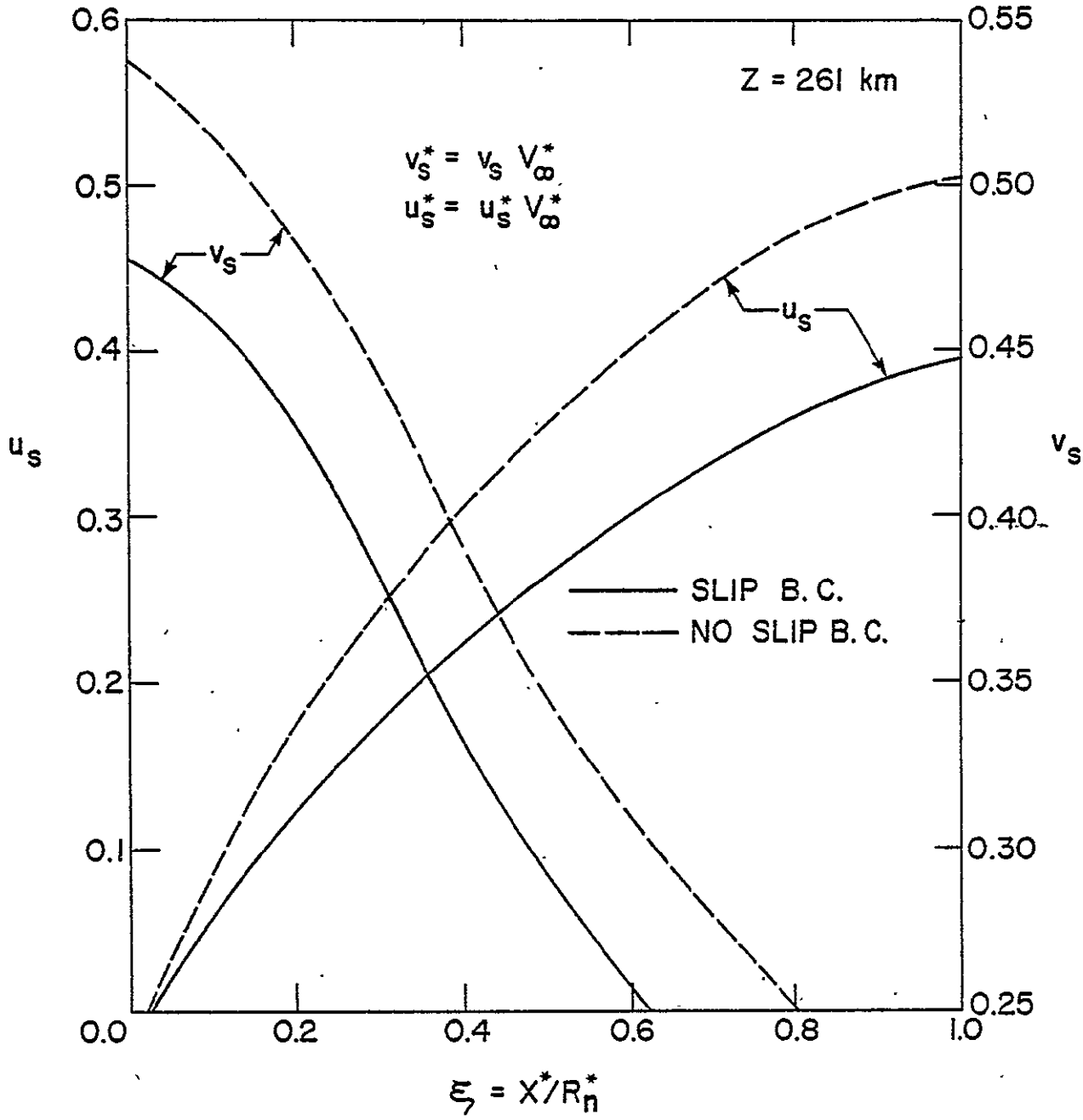

Figure 6. Velocity variation (just behind the shock wave) as a function of ξ-coordinate.

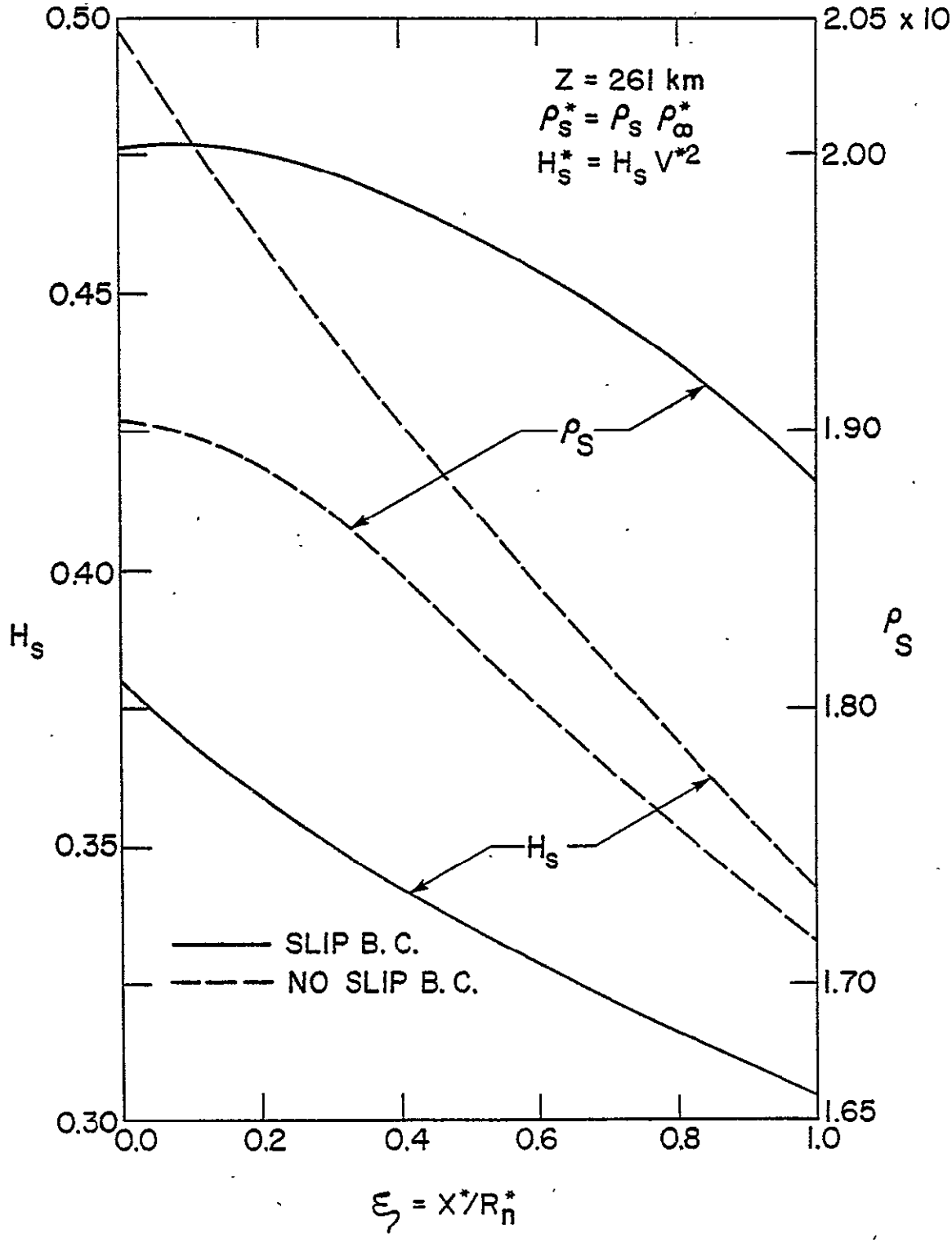

Figure 7. Total enthalpy and density variation (just behind the shock wave) as a function of ξ-coordinate.

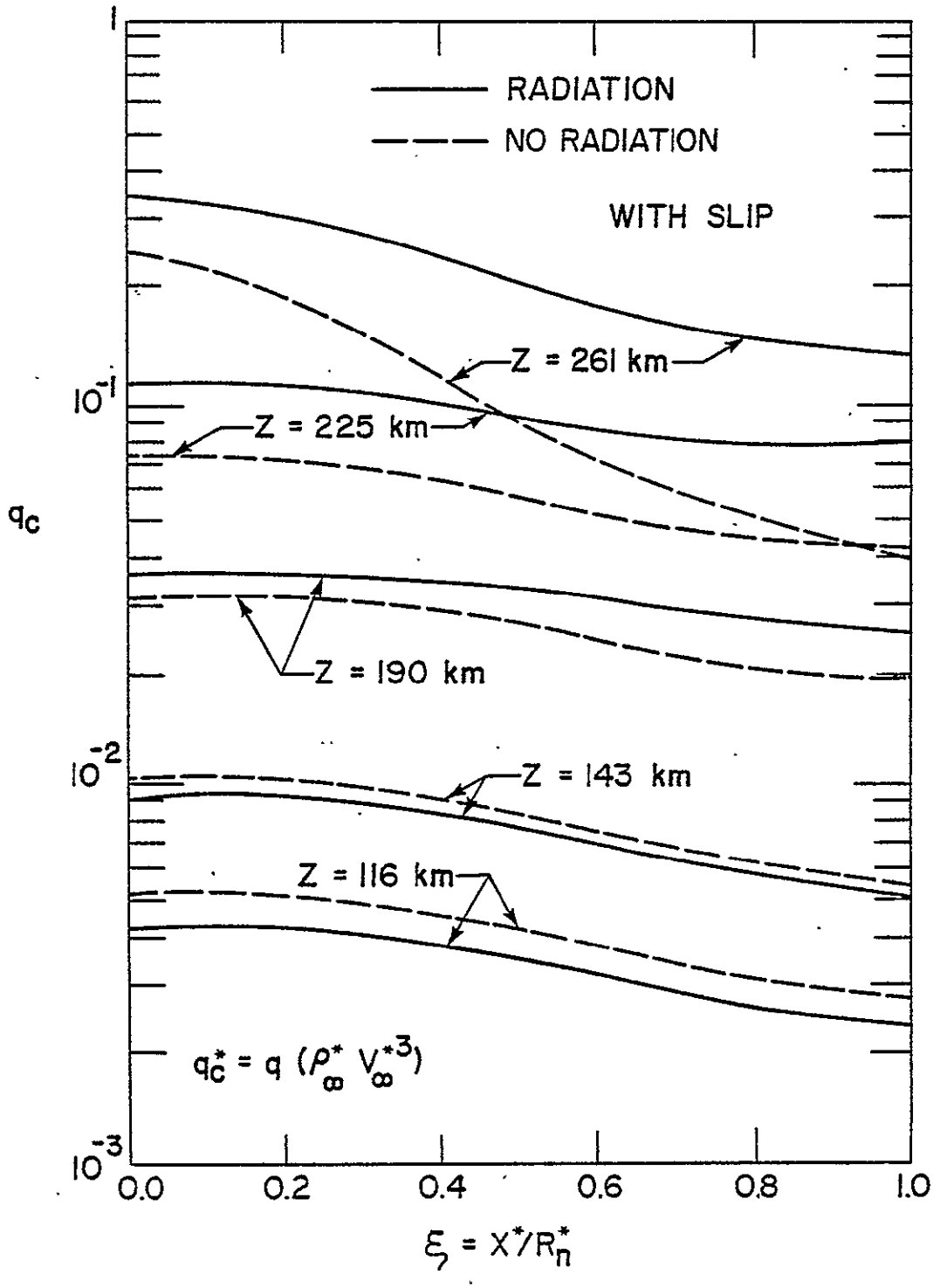

Figure 8. Effects of the radiative heat flux to the convective heat flux along the body surface.

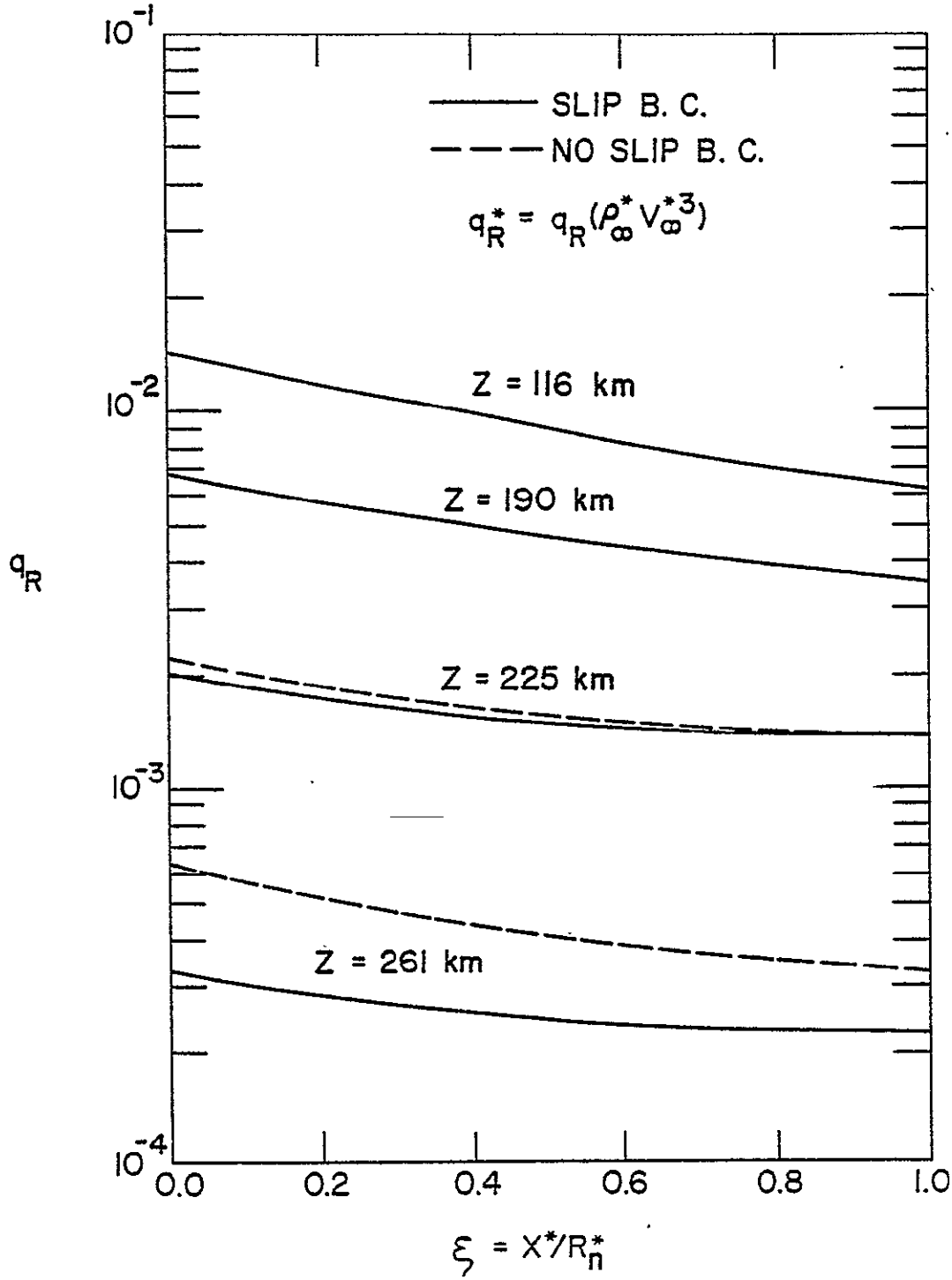

Figure 9. Comparison of slip and no-slip results for radiative heat-flux variation along the body surface.

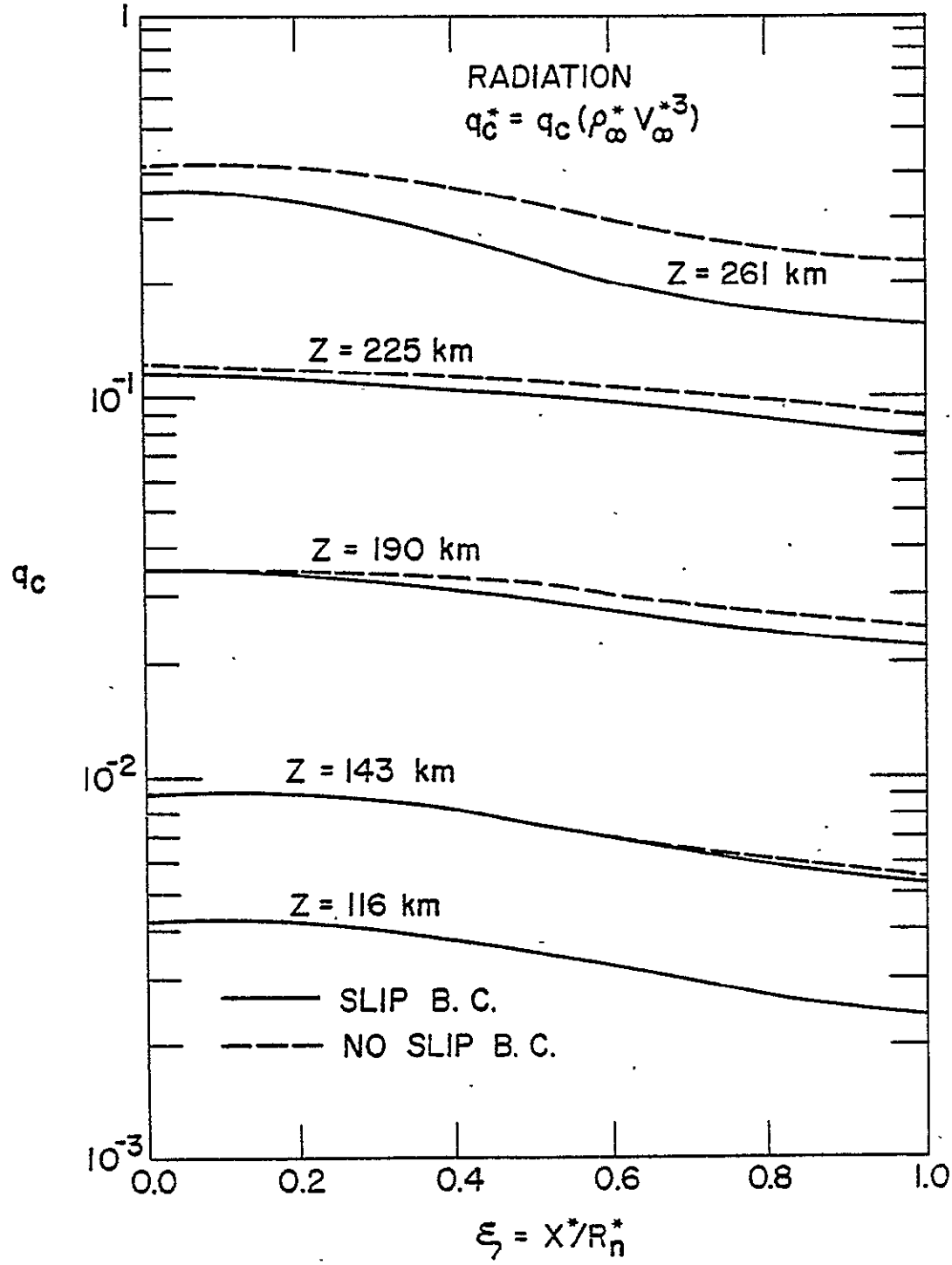

Figure 10. Comparison of slip and no-slip results for convective heat-flux variation along the body surface (with radiation).

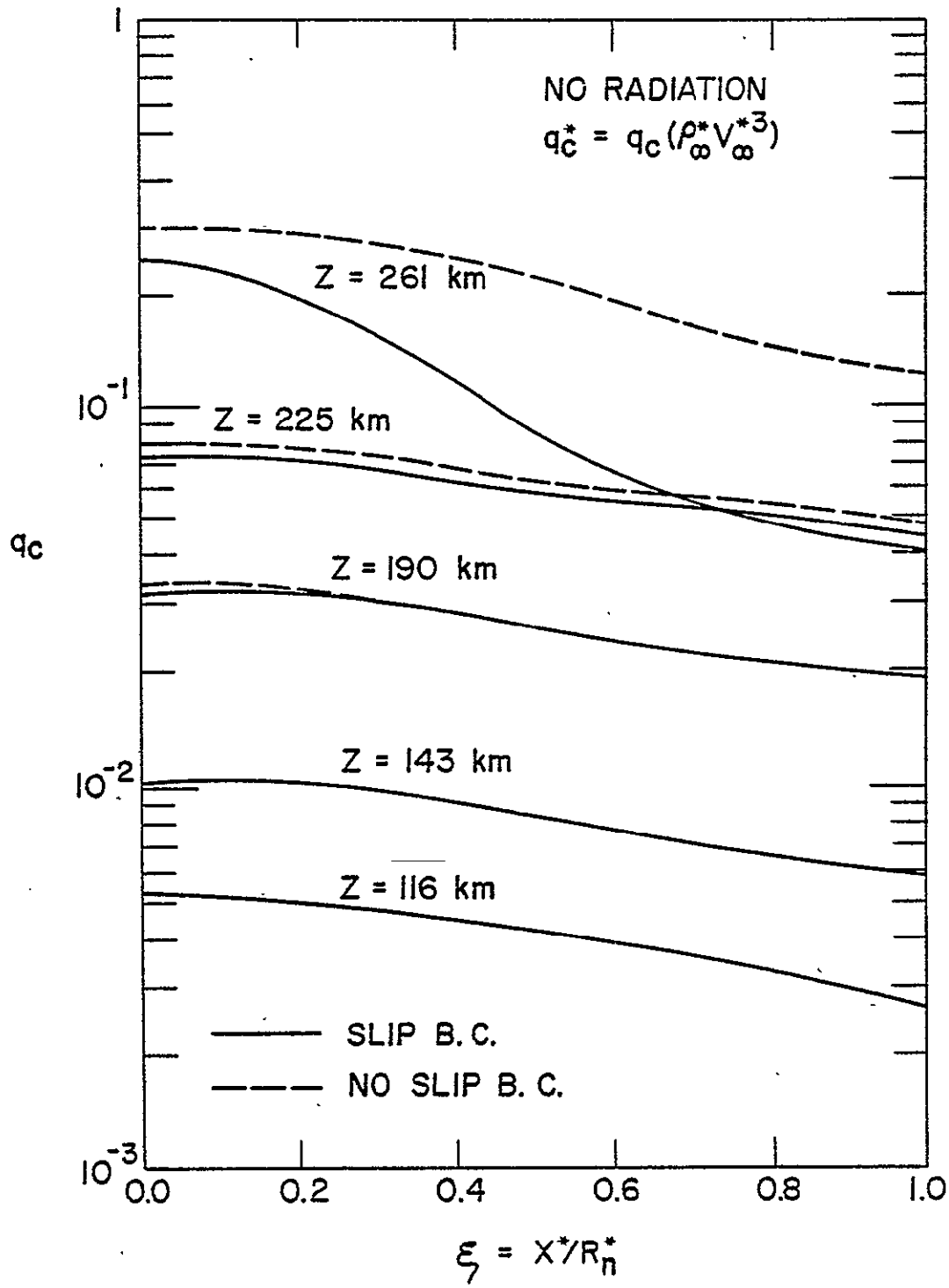

Figure 11. Comparison of slip and no-slip results for convective heat-flux variation along the body surface (with no radiation).